Nanoscale

REVIEW

View Article Online
View Journal | View Issue

Cite this: *Nanoscale*, 2017, **9**, 7320

Group III nitride nanomaterials for biosensing

Xiao Li[a,b] and Xinyu Liu*[a]

Received 4th March 2017,
Accepted 1st April 2017

DOI: 10.1039/c7nr01577a

rsc.li/nanoscale

Biosensing has found wide applications in biological and medical research, and in clinical diagnosis, environmental monitoring and other analytical tasks. Recognized as novel and outstanding transducing materials because of their superior and unique physical/chemical properties, group III nitride (III–nitride) nanomaterials have been introduced into biosensor development with remarkable advancements achieved in the past few decades. This paper presents the first comprehensive review on biosensor development with III–nitride nanomaterials. The review starts with the introduction of the material properties and biocompatibility of III–nitrides that are useful for biosensing. The focus is then placed on surface treatments of III–nitrides, which lay the foundation for biosensing, and on biosensing mechanisms where the exceptional properties of III–nitride nanomaterials lead to superior biosensing performance. From a practical point of view, techniques for biosensor fabrication are then summarized. Finally, existing biosensing applications and future directions are discussed.

1. Introduction

Biosensing is an important technology for biological and medical research,[1] and has many real-world applications such as medical diagnosis,[2] security surveillance,[3] and environmental monitoring.[4] A biosensor usually converts the existence, characteristics, and/or behavior of a biologically relevant analyte into measurable signals. The target analytes range from simple molecules such as hydrogen ions (H^+) to complex ones such as proteins and deoxyribonucleic acids (DNAs) and to living cells and organisms such as cancer cells and bacteria. The detectable characteristics of an analyte could be a functional group, electrical charge, protein conformation, and so forth. The behaviors related to an analyte of interest may be charge transfer, biomolecule movement, intermolecular force, and so forth. The measurable signals in biosensors are mostly electrical signals such as current, potential, capacitance and conductance. Mechanical and optical signals can also be transduced from the target markers.

The transducing material in a biosensor is the essential component that enables the biosensing functionality, and should meet several central requirements to be effective in real applications: (i) it should be easy to functionalize with sensing probes, to allow specific recognition and/or reaction with the target markers; (ii) it must provide sufficient accuracy and sensitivity; (iii) it should also maintain a reasonable cost; (iv) it is expected to function stably in its working environment, which could be complex and harsh; (v) if the application involves direct handling of living samples (*e.g.*, cells and micro-organisms), it should not impose considerable injurious effect on the samples.

The utilization of nanomaterials as the transducing materials has sparked unprecedented advancements in biosensing research over the past few decades,[5–8] as the unique phenomena at the nanoscale grant nanomaterials highly desirable properties for biosensing. Charge carriers in nanomaterials are limited and close to the interfaces to the sensing environment, and thus the presence of target markers may significantly affect the accumulation or depletion of the carriers, generating drastic electrical signal changes. Nanomaterials commonly have high surface energy and high surface-to-volume ratios, and thus can capture more target markers, resulting in high sensitivity. Nanomaterials are often formed through a bottom-up growth process, which gives them critical advantages over conventional top-down fabrication processes, for example, superior resolution down to the atomic level, and ease of doping and achieving a heterogeneous composition.[9]

Nanomaterials of group III nitrides (or simply III–nitrides) have more attractive characteristics than what are commonly shared among nanomaterials to serve as the transducing materials in biosensors. This class of materials typically include gallium nitride (GaN), aluminium nitride (AlN), indium nitride (InN), and their alloys. They have electrical and optical properties widely tunable by the crystal lattice structure, alloy composition, heterostructure, and dopant, to match demanding biosensor designs. As wide-bandgap semiconducting materials, they are often capable of operating at high voltage, high frequency and high temperature, to support more

[a]*Department of Mechanical Engineering, McGill University, Montreal, Quebec H3A 0C3, Canada. E-mail: xinyu.liu@mcgill.ca*
[b]*Department of Chemistry, Stanford University, Stanford, California 94305, USA*

powerful electrical mechanisms in biosensor construction. They also have high chemical and thermal stability to work under harsh sensing environments. Some III–nitride nanomaterials (*e.g.*, aluminium gallium nitride/gallium nitride—AlGaN/GaN—heterostructure) have high electron mobility and high electron sheet concentration, making them more sensitive to the target markers. High stiffness and correspondingly high resonance frequency are other characteristics of some III–nitride nanomaterials, which could be utilized in high-sensitivity mechanical biosensing. Alongside these intrinsic features, the development of technologies for synthesis and device-level integration of III–nitride nanomaterials is another major driving force in the substantial research progress of III–nitride nanomaterial based biosensors in the past and at present.[10,11]

Several reviews have been published discussing the syntheses, properties, and applications of III–nitride nanomaterials, and some of them touch on some biosensing applications of III–nitride nanomaterials.[12–14] However, to the best of our knowledge, there is no comprehensive review dedicated to the biosensing-related technologies, methodologies and applications of III–nitride nanomaterials. In this article, we present a comprehensive review on III–nitride nanomaterials for biosensing. We first summarize the major properties of III–nitride nanomaterials and their merits in biosensing. As the essential parts that distinguish this review from previous ones, systematic reviews in great detail are presented with regard to the surface functionalization routes, biosensing mechanisms, biosensor fabrication and applications of III–nitride nanomaterial based biosensing. In particular, compared to a previous review on III–nitride-based electronic biosensors,[14] this review covers all types of existing III–nitride biosensors based on electronic, optical and mechanical sensing mechanisms, and discusses important technological aspects of these devices. Thus we believe that the thorough methodologies and technical details organized in this review will provide guidelines to boost the development of III–nitride nanobiosensors.

2. Material properties of III–nitrides

III–nitrides have three crystal structures: zinc blende, rock salt, and wurtzite. The former two have cubic unit cells, whereas the wurtzite structure has hexagonal uniaxial anisotropy unit cells as shown in Fig. 1, taking GaN as an example.[11] The wurtzite structure is the major crystal structure of III–nitride nanomaterials reported in the literature; thus, only III–nitride nanomaterials with the wurtzite structure will be discussed in the following sections.

The growth direction of III–nitrides is usually normal to alternating {0001} planes consisting of anions or cations. The non-centrosymmetric hexagonal structure determines that III–nitrides have polarities (Fig. 1).[11] Polarity is a bulk property, while the surface of III–nitride materials could be terminated with anions or cations. The polarity and surface termination of the III–nitride nanomaterials could affect the biosensing-related properties.

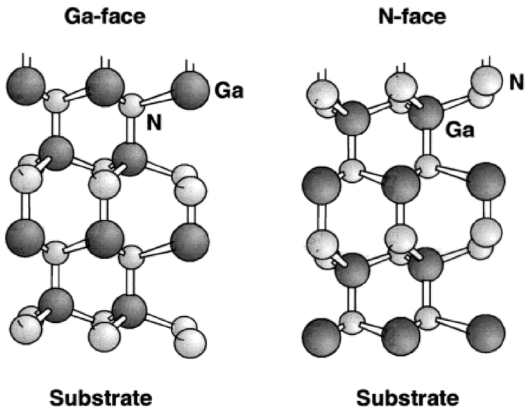

Fig. 1 Wurtzite unit cell of GaN crystals. The illustration shows wurtzite structures of GaN with two polarities. "Ga-face" means the gallium plane is on the top of the {0001} biplane consisting of the closest gallium and nitrogen planes.[16] "N-face" means the nitrogen plane is on the top of the {0001} biplane. Reprinted and adapted with permission from ref. 16, Copyright 1999, IOP publishing. DOI: 10.1088/0022-3727/31/20/001.

In the wurtzite structure, there are pairs of cations and anions attracting each other by electrostatic force, along the [0001] direction. It shortens the distance in each pair and this deformation induces spontaneous polarization, which is larger than that in many other materials.[11,15] Spontaneous polarization contributes to the generation of a two-dimensional electron gas (2DEG) in AlGaN/GaN heterostructures, which is close to the nanomaterial surface and very sensitive to any change in its proximity.

Although sharing some common properties, each of the well-studied III–nitrides has shown distinct features that are valuable to biosensing. III–nitrides are direct semiconductors, and their bandgaps range from 0.64 eV for InN to 3.4 eV for GaN and to 6.2 eV for AlN.[16] Therefore, III–nitrides cover a wide spectrum from near infrared (IR) to ultraviolet (UV), which has sparked enormous research interest in III–nitrides for light emission,[16] as well as photodetection,[17,18] both of which can be utilized in optical biosensing. GaN is the most studied III–nitride material and is known for its extraordinary stability to moisture, high temperature and chemicals.[11] AlN possesses high stability like GaN, with a high piezoelectric effect and electromechanical coupling coefficient.[19,20] InN has a narrower bandgap compared to GaN and AlN, but it is still a very stable material. An interesting feature of InN is its very large surface charge due to its surface carrier accumulation,[21] which makes it a candidate transducing material for ultrasensitive sensors.[22] Even more, the lattice constant and bandgap can be readily tuned by III–nitride tertiary alloys with various ratios, leading to widely controllable properties.[11]

3. Biocompatibility of III–nitrides

When biosensors directly deal with living organisms such as human bodies, micro-organisms and cells, the biocompati-

bility of the transducing materials is a critical concern. GaN has proven its high biocompatibility in different reports. In comparison to silicon, GaN shows better biocompatibility in cerebellar granule neuron culture and better support to neurite network formation and neurite outgrowth.[23] A more comprehensive study was conducted on GaN surfaces using fibroblasts in the radiation biophysics context.[24] Observations and quantifications of cell proliferation and growth, as well as DNA repair after ionizing radiation, implied good biocompatibility and biofunctionality at the cell–GaN interface. On the other hand, nanoparticles are often used in antibacterial applications, and thus their toxicity may raise a concern in biosensing. Prasana Sahoo *et al.* have reported a study on the toxicity of GaN nanoparticles (NPs) to bacteria cells.[25] Above 80% inhibition of bacterial biofilms was observed, and confocal Raman spectroscopy revealed bacterial membrane damage possibly caused by sorption and passive intake of the GaN NPs.

Aluminium (Al) is known for its toxicity,[26,27] and its toxic effect was interrogated in some research studies with the III–nitrides that contain Al element. In an earlier study, oxidized and non-oxidized surfaces of GaN, AlN, and $Al_{0.22}Ga_{0.78}N$ were tested by culturing fibroblasts for over 24 hours.[28] Cells retained their vitality on both the oxidized and non-oxidized surfaces, evidenced by cell density measurements and morphology observation. In particular, Al content in AlGaN did not have appreciable effects on the cells, accredited to the formation of a thin film of chemically robust metal oxide on the surface. A more recent study performed comprehensive evaluations on the attachment, proliferation, and mortality of human embryonic kidney 293 cells cultured on AlGaN/GaN heterostructures without any surface treatment. The $Al_xGa_{1-x}N$ surface showed favourable results in these aspects of biocompatibility in a certain range of composition (x = 0–0.35), while the GaN cap (x = 0) over the heterostructure improved the overall biocompatibility of the material.[29] However, as the study found out, increased Al content in AlGaN resulted in slower proliferation and slightly higher death rate of the cells. Therefore, the reports published so far indicate the necessity of investigating the behaviour and function of specific cells involved in biosensing with Al content. There are also surface treatment approaches available for improving biocompatibility as we will discuss in the next section.

4. Surface treatment

The surfaces of III–nitride nanomaterials, which directly interact with target analytes, play a pivotal role in biosensing. Proper treatment of the material surface is required to achieve superior biosensing performance. Here, we categorize the reported surface treatment techniques for III–nitrides into two groups: surface property tuning and biofunctionalization. In the group of "surface property tuning", we introduce the techniques for tuning the surface properties of III–nitrides for biosensing. In the group of "biofunctionalization", we present the techniques for introducing probe molecules on III–nitride surfaces through a series of chemical modifications, which allow the biosensors to capture and detect specific target markers.

4.1 Surface property tuning

Through chemical or physical treatments, it is possible to tune the surface properties of III–nitride nanomaterials, which affect their biosensing performance. Surface properties normally concerning biosensing are electrical properties, wettability, and biocompatibility. The electrical properties of III–nitrides influence the quality of electrical readouts (*e.g.*, signal-to-noise ratio and drifting) of the biosensors, and might also be associated with the material's essential sensing capabilities like sensitivity. Wettability (*i.e.*, level of hydrophilicity) is an effective method for tuning the biosensing performance, given that most analytes in biosensing are detected in liquids. In general, a hydrophilic surface of the transducing material allows the liquid to deliver the target analytes extensively over the contact area of the material surface and thus induces more detectable changes, which can eventually improve the sensitivity and limit of detection (LOD) of the biosensor. On the other hand, hydrophobicity leads to nonspecific adsorption of proteins, which is generally undesirable.[30] However, superhydrophobicity could potentially be employed to perform self-cleaning or other functionalities on sensor devices.[31] High biocompatibility is usually beneficial, as mentioned above, to applications that involve cell/organism culture or close contact of the material/device with human bodies.

One way to modify the electrical properties of III–nitrides is to treat the material surface with specific solvents. InN has strong surface charge accumulation, and researchers found that the surface carrier density and mobility of InN could be enhanced through surface treatment using solvents such as methanol and water.[22] The enhancement was found to be specific to the type of solvent, and took effect rapidly upon treatment and decayed at low rates. The origin of the enhancement might be the interaction between the dipole molecules and the surface states of III–nitrides. This phenomenon can be used for improving the sensitivity of III–nitrides, because carriers accumulated close to the material surface could potentially respond to the target marker more drastically.

The wettability of III–nitrides can be improved through oxidation. For example, the water contact angle of the as-grown $Al_{0.30}Ga_{0.70}N$ surface with native oxide is approximately 89°. Researchers found that the water contact angle decreased to about 5° right after wet or dry oxidation, and finally stabilized at 42° after being stored in air for a few days.[32] In this report, wet and dry oxidations generated similar results on the contact angle, but the latter was completed through a rapid thermal process which took much shorter time. A more comprehensive comparison of contact angle changes after different oxidation processes could be found in another report where researchers have investigated three oxidation approaches on the surface of N-face and Ga-face GaN, including wet and dry thermal oxidations, and H_2O_2 chemical oxidation.[28] The researchers experimentally confirmed that both dry and wet thermal

oxidations within the range of 650–750 °C generated the smallest contact angles. Sometimes, III–nitrides are required to be hydrophobic, which confines the sensing area. The fluorocarbon film could be grown to serve as the inert layer, but its effect decays within a few hours.[32] A more recent study highlighted the importance of appropriate morphological features in generating the super-hydrophobic surface, and the authors combined different surface morphologies, obtained with wet etching, with different chemical surface treatments to tune the hydrophilicity *vs.* hydrophobicity of GaN surfaces.[33] Whisker-like morphology generally made the surface much more hydrophobic, and the contact angle of water became higher than 150° when the surface was sputtered with gold and subsequently bonded with $C_{18}SH$ thiol. However, a bare gold coating on whisker-like morphology made the surface drastically hydrophilic due to the favorable capillary forces. In addition, the controllable wettability may bring extra functionalities to the sensing system. Li *et al.* explored the feasibility of changing the surface of photoresponsive GaN nanowires (NWs) from superhydrophobicity to superhydrophilicity by UV illumination.[34] Correspondingly, protein absorption and cellular adhesion were modulated on the surface.

Previous reports have shown decent biocompatibility of III–nitrides independent of the surface oxidation process as mentioned above, and certain surface modifications could favor the interaction between III–nitrides and living organisms. For example, researchers modified the GaN surface with a cellular-adhesion-promoting IKVAV peptide, and found better spreading of PC12 cells on the surface-modified material, along with flattened cell bodies and increased microvilli growth.[35] A later study compared methods of attaching the IKVAV peptide.[36] The peptide molecules were either covalently linked to the GaN surface or contained a motif to recognize the GaN surface and perform affinity attachment. It was found that covalent attachment promoted monolayer and dispersed P12 cell adhesion, and affinity-driven attachment promoted multilayer P12 cell agglomeration. This discovery would allow for preferential tuning of GaN biocompatibility in sensing applications. The surface topology of III–nitride, when combined with a physically absorbed IKVAV peptide, was also found to play an important role to influence cellular adhesion and differentiation.[37] As mentioned above, changing the wettability of III–nitride may affect cellular adhesion and survival.[38,39]

Besides the purposeful surface modifications, some modifications could also be made collaterally over the processes for device preparation and fabrication, such as heating, cleaning, etching for creating structures, sterilization for culturing cells, passivation for protecting electrodes, and so forth. For example, the carrier density in the 2DEG of AlGaN/GaN heterostructures was decreased because of the thermal degradation effect in the process of oxidation.[32] A series of tests on these typical processing steps for constructing electrical sensors were reported, using AlGaN/GaN heterostructures with a GaN cap layer as the model.[40] The process involved HF and HCl cleaning, KOH wet etching, Cl_2 and SF_6 plasma etching, autoclaving (for sterilization), and polyimide coating (for passivation). In general, the processing steps were found to affect cell growth on the sensors to a small extent. Autoclaving increased the contact angle of the material surface, while the other steps changed the contact angle temporarily but it recovered to its initial value of 50° after a few hours. Certain steps were found to bring contaminations, which affected the surface morphology and influenced the electrical properties. Readers may refer to ref. 40 for more details of the changes caused by each of the steps. In a more recent study focused on the etching process, Wilkins *et al.* discovered that phosphoric acids added into the process affected GaN in such aspects as wettability, photoluminescence (PL) emission, and oxide formation.[41] A series of X-ray photoelectron spectroscopy (XPS) investigations undertaken by Khir *et al.* offered explanations on the varied AlGaN/GaN ionic sensing performance in reports by revealing the altered ionic affinities of AlGaN and GaN subjected to oxide growth and chemical treatments.[42] These studies offer insights for deliberate sensor preparations.

4.2 Surface biofunctionalization

Surface biofunctionalization is the foundation for specificity in biosensing, through which probe molecules are immobilized on the surface of transducing material. In biosensing, the probe molecules specifically capture the target markers typically based on immunological recognition of proteins and hybridization of DNAs. Linking molecules may be necessary to connect the surface of transducing material with the probe molecules through various types of physisorption or chemisorption, among which covalent bonding is preferable because it is more stable and selective than other types of connections. An important consideration in covalent biofunctionalization of semiconductor nanomaterials is the compatibility between the bands (valence band maximum and conductance band maximum) of the semiconductors with the electrical levels (highest occupied molecular orbitals—HOMO, and lowest unoccupied molecular orbitals—LUMO) of the biomolecules to be conjugated. In this regard, the bands of III–nitrides match well the HOMOs/LUMOs of typical biomolecules (*e.g.*, proteins and DNAs).[13,43]

4.2.1 Organosilane-based biofunctionalization. One of the most widely used approaches for covalent bonding between biomolecules and the surfaces of semiconductors (including III–nitrides) is based on organosilane linking molecules.[43,44] The superior reproducibility of organosilane-based protein functionalization over physisorption-based ones is evident in biofunctionalization of III–nitrides.[45] A typical process of organosilane-based biofunctionalization follows three steps. (i) The III–nitride surface is first hydroxylated or oxidized. (ii) An organosilane (*e.g.*, aminopropyltrimethoxysilane—APTMS, 3-aminopropyltriethoxysilane—APTES, or 3-mercaptopropyltrimethoxysilane—MPTMS) is then covalently bonded with the hydroxyl groups (–OH) or oxygen atoms (=O) on the surface. (iii) The probe molecule is immobilized eventually; sometimes another linking molecule is introduced between the organosilane and the probe molecule (*e.g.*, glutaraldehyde—GA). Considering its prevalence in III–nitride biosensing, we discuss the step-by-step technical

details of organosilane-based biofunctionalization and its characterization techniques.

As the first step, –OH or =O is introduced on the surfaces of III–nitrides through treatment in a piranha solution (H_2SO_4/H_2O_2),[46] an acid mixture (H_2SO_4/HNO_3),[47] or oxygen/air plasma (Fig. 2).[48] –OH and =O are often coupled, as the former could evolve from the latter. The oxidation treatments may affect the properties (*e.g.*, wettability and carrier density[32]) of III–nitrides, as discussed in the section "Surface property tuning", and Wen *et al.* have compared different oxidation processes as part of the biofunctionalization procedure on AlGaN surfaces of AlGaN/GaN heterostructures for the preparation of a protein sensor.[49] Inductively coupled oxygen plasma was found to be superior, in terms of protein binding efficiency, compared with reactive ion etching oxygen plasma, inductively coupled oxygen plasma, and piranha solution, mainly; this was confirmed by fluorescence observation and enzyme-linked immunosorbent assays (ELISAs).

When organosilanes are introduced onto the transducer surface, stable transducer–O–Si bonds are formed, leaving specific terminal groups for the subsequent linking. One needs to properly choose the exposed terminal groups of organosilanes, because the terminal groups should be able to bond with the molecules introduced subsequently. There are two popular terminal groups used for surface biofunctionalization of III–nitrides: amine group (–NH_2; as in the case of APTMS and APTES) and thiol group (–SH; as in the case of MPTMS) (Fig. 2). Different bonding mechanisms related to each of the two terminal groups will be explained later in this section.

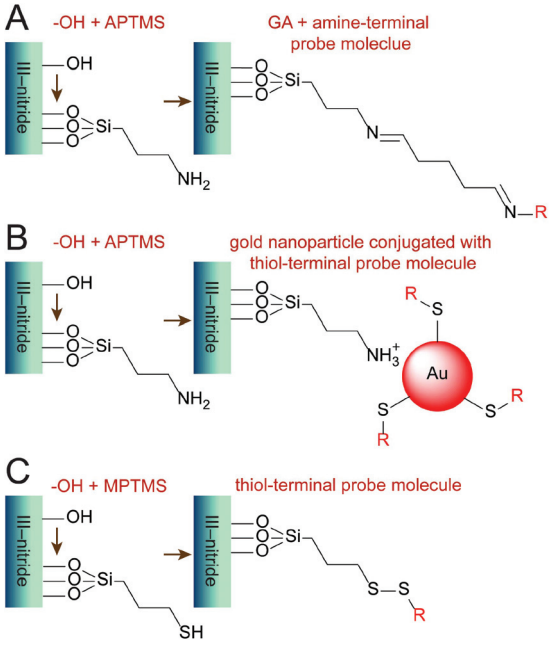

Fig. 2 Typical chemical processes of organosilane-based biofunctionalization. In the schematics, "R" represents probe molecules or other functional molecules.

Besides providing linkers for molecular conjugation, the introduction of organosilane may also alter the physical properties of III–nitride nanomaterials. In electrochemical characterization of working electrodes made from GaN NWs, wide potential windows, low background current density levels and high oxidation current peaks were registered with the MPTMS modification.[50] However, the existence of MPTMS hinders efficient transfer of electrons from the analyte to the NWs, leading to slow kinetics in electrochemical biosensing. In optical characterization, concentration-dependent effects of the organosilane layer were observed with GaN NWs upon MPTMS functionalization.[47] Surface treatment using low-concentration MPTMS generated blue shift, increased intensity and narrower emission linewidth in PL tests. However, excessive treatment with MPTMS resulted in a reversed effect which increased the bandwidth and decreased the emission intensity, because MPTMS also absorbed photons.[47] It should be noted that the surface properties of the III–nitride material affect the quality of biofunctionalization. Arranz *et al.* showed that through the same organosilane-based biofunctionalization, p-type GaN ended up with a monolayer of APTES at a coverage of up to 78%, whereas n-type GaN was coated with approximately three layers thick APTES.[51] That was because the available hydroxyl group density of n-type GaN after the hydroxylation step was lower than that of p-type GaN. The low-density hydroxyl groups could not allow all three ethoxy groups (–OCH_3) of an APTES molecule to form transducer–O–Si bonds directly on the surface of GaN, and some groups of APTES molecules react with each other to form Si–O–Si bonds, generating the thick APTMS layers. The high coverage rate of the organosilane monolayer is generally favorable for sensitivity enhancement in electrical sensing, as it provides more bonding sites for target markers and a shorter distance from the marker to the transducer.

Following the immobilization of organosilane on the III–nitride surface, probe molecules can be introduced (Fig. 2). Probe molecules are typically antibody/antigen proteins or single-stranded DNAs that are specific to the target biomarkers, and the probe molecule could covalently bond with the functional groups of the organosilane by either introducing a linker molecule in between or modifying the probe molecules themselves before immobilization (*e.g.*, adding amine or thiol groups), and sometimes both are needed. For the organosilanes terminating with amine groups (*i.e.*, aminosilanes), GA is widely used as the linker molecule because it can readily bond, through the reductive amination, with the amine groups of both aminosilane and probe molecule (*e.g.*, proteins and amine-group-modified DNAs) (Fig. 2A).[45,52–54] Another method to bond aminosilane with DNA is based on electrostatic attraction between –NH_3^+ of the aminosilane and negatively charged gold nanoparticles (AuNPs), where thiolated oligonucleotides were pre-conjugated with the AuNPs (Fig. 2B).[55] Besides these two common processes, researchers utilized the bond between an amine group and a sulfonyl group to tag luminescent Ru(II) polyazaheterocyclic (an oxygen

indicator) with APTES.[46,56] For organosilanes terminating with thiol groups (*i.e.*, thiolsilanes), S–S bonds could be established between the thiol groups of both thiolsilane and thiol-modified DNAs (Fig. 2C).[50] Besides aminosilanes and thiolsilanes, researchers also succeeded in functionalizing GaN and AlN with methyl-terminated organosilane that has a long alkyl chain (octadecyltrimethoxysilane—ODTMS);[52,57] thus, it is possible to use the methyl functional group and the alkyl chain to form lipid membranes.

A notable concern in biofunctionalization is the distance between the immobilized probe molecules and the surface of the transducer. Although short distance generally yields better sensitivity because of the close interaction of the target marker with the transducer surface, the bioactivity of the functional molecules might be compromised due to steric hindrance, which might lower the efficiency of capturing target biomarkers. Cao *et al.* investigated different spacers linking organosilane with silicon wafer, for the interactions with *Escherichia coli* (*E. coli*) and antibody molecules on the wafer surface.[58] Atomic force microscopy (AFM) revealed that the strongest probe–analyte interaction was achieved using the spacer Jeffamine® ED-600 (J600), and the conjugation efficiency and bonding force could be adjusted by the length of the spacer. This spacer was used in biofunctionalization on the AlN surface in another report.[59]

4.2.2 Alternative biofunctionalization methods. Although organosilane-based biofunctionalization is widely used in biosensing, its process is often extensive and the formation of organosilane thin-films is prone to inconsistency, because the water concentration largely affects the polymerization rate.[60,61] There are a number of other biofunctionalization methods developed for III–nitrides, which complement the organosilane-based methods and could lead to more convenient biofunctionalizaiton and higher performance of III–nitride-based biosensing. We categorize these methods into three groups: (i) replacing organosilanes with other chemicals to build the bonds; (ii) directly introducing functional groups on the III–nitride surfaces that bond with the probe molecules; (iii) directly forming the probe layer on the III–nitride surfaces. We introduce the reported techniques for each of the strategies in this section.

Replacing organosilanes with other chemicals to build the linkages. One method is based on the well-studied thiol–Au bonding. Gold thin-films can be deposited onto III–nitride surfaces, and then thiol-terminated organic molecules can be self-assembled on the gold surface (Fig. 3A). For example, thioglycolic acid was used as a linker between gold films and probe molecules, because it features a thiol group and a carboxyl group (–COOH), the latter of which can be converted into carboxylate succinimidyl ester to further bond a ligand specific for prostate specific antigen.[62] It can also be linked with amine groups of other antibodies.[63–66] In another report, a chemical receptor, where a boronic-acid-containing group and a thiol group were bridged by an alkane chain, was synthesized and bonded to a gold film on the AlGaN/GaN heterostructure, and the boronic acid containing group is the probe for saccharides.[67]

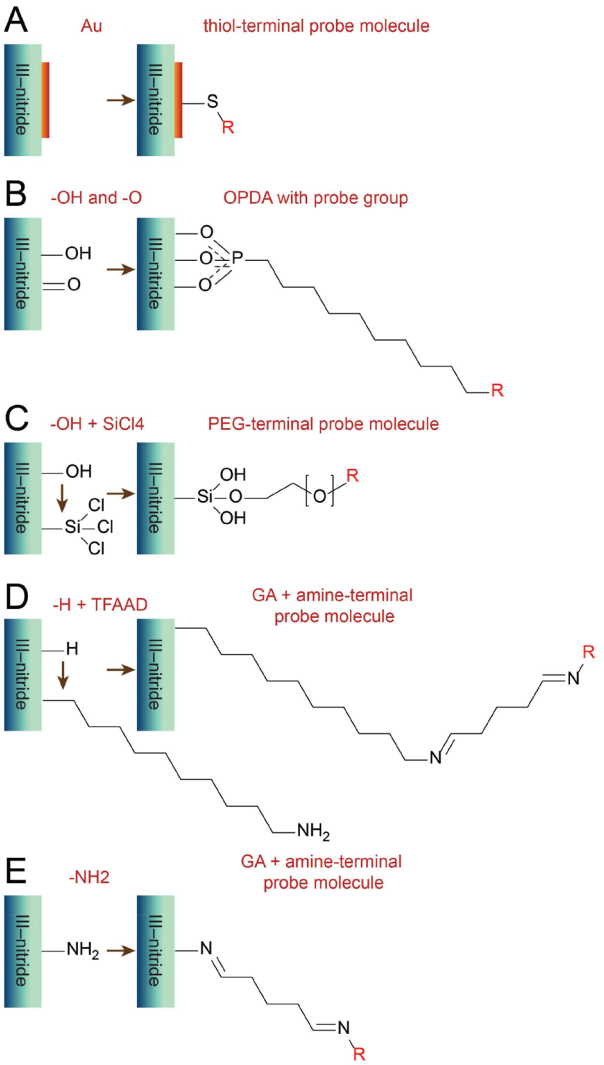

Fig. 3 Alternative biofunctionalization methods. In the schematics, "R" represents probe molecules or other functional molecules.

Researchers have proposed organophosphonic acid (*i.e.*, octadecylphosphonic acid—OPDA) as another substitute to organosilane, and it was formed on GaN and AlGaN as a densely packed layer,[68–70] after the surfaces were oxidized by UV light exposure in ozone or air (Fig. 3B). Alternative hydrocarbons with terminal groups like –COOH, –OH, –SH, and $-NH_2$ were found to weakly attach to GaN surfaces, implying that organosphonic acids may be used to introduce these groups to III–nitride surfaces and leave these terminal groups available for subsequent bonding with functional molecules.[68] Electrical analyses revealed that the AlGaN/GaN heterostructure retained its channel conductivity when organosphonic layers existed,[70] but their desorption from the substrate was observed in aqueous solution,[68] especially when the solution was basic.[69] In a subsequent study, UV-initiated polymerization of layers of diacetylenic alkylphosphonic acids on GaN and AlGaN surfaces was found to have better stability in NaOH

solution, but with less uniform coverage due to light blockage at the step edges and UV-induced degradation.[71]

Silicon tetrachloride ($SiCl_4$) was used to replace organosilane, also generating a transducer–O–Si bond. Atomic layer deposition (ALP) using water as the oxygen source was first used to generate hydroxyl (–OH) groups on GaN NWs (Fig. 3C).[72] Al_2O_3, TiO_2 and SiO_2 nano-films were formed by ALP, and the hydroxyl group density obtained was several times higher than that obtained through piranha solution treatment. The reaction of –OH and $SiCl_4$ generated transducer–O–Si bonding, leaving Si–Cl available to bond with poly (ethylene glycol)–biotin (PEG-biotin). High-efficiency streptavidin capture (by biotin) was achieved subsequently.

Another competent linking group that could replace organosilane in III–nitride biofunctionalization is the alkene group. One approach is to let alkene groups react with hydrogen on the GaN surface under 254 nm light. Researchers prepared a so-called "TFAAD" molecule that has ω-unsaturated amine 10-aminodec-1-ene protected with the trifluoroacetamide functional group.[73] This molecule, which has a alkene terminal and a protected amine terminal, could bond to the GaN surface, and the amine terminal was capable of linking thiol-modified DNAs with the assistance of another linking molecule (Fig. 3D). Another approach is to form alkene groups on the GaN surface. Researchers have successfully functionalized the (0001) surface of GaN by sequentially introducing hydrogen, chlorine, and alkene groups.[74] The alkene groups were used to introduce functional groups (*e.g.*, –COOH) through olefin metathesis. Furthermore, hexylamine or a peptide bound to –COOH.

Directly introducing linking groups on the III–nitride surface. $-NH_2$ is often the key linking group to immobilize probe molecules, and Stine *et al.* have directly generated $-NH_2$ on the GaN surface upon humid air plasma treatment.[60] Then, GA could be used for protein binding, and the bulk conductivity of GaN was only changed slightly after this treatment (Fig. 3E). The possible origin of the directly formed amine groups is the breakdown of Ga–N bonds followed by the formation of Ga–O and N–H bonds. In theory, the upper limit of the amine group coverage is 33% with humid plasma treatment,[60] lower than the up to 78% coverage reached in organosilane-based approaches.[51]

Directly forming a probe layer on the III–nitride surface. Research efforts have also been made to directly form probe molecules on III–nitride surfaces and eliminate the tedious biofunctionalization procedures. Lipid membranes can be deposited on oxidized AlGaN and GaN surfaces through incubation, to form ion-selective channels for electrochemical sensing.[28,75] Phage display was used to evolve a peptide specific to GaN,[76] and this peptide could be further functionalized (*e.g.*, through biotinylation) to specifically recognize target biomolecules. DNAs have been successfully printed on the cleaned AlGaN surface directly, and strong attachment was achieved between the 5′ phosphate group of the DNAs and the oxide layer of the AlGaN.[77] Furthermore, Li *et al.* demonstrated that the combination of a GaN affinitive peptide and a tumor specific DNA aptamer could generate a GaN-NW surface that captures and releases cancer cells.[78] Deoxyguanosine was used for DNA binding on GaN quantum dot surfaces and was supposed to provide some advantages because they share similar optical properties.[79] However, when shortening the linking distance by the above methods, one should consider possible negative effects arising from the steric hindrance, as discussed in the section "Organosilane-based biofunctionalizaiton".

4.2.3 Patterning biofunctionalization. Patterning of functional molecules is required for certain types of applications such as multiplexed detection of several target markers in selected regions of a sensor (usually on thin films). Photolithography is one of the popular methods for molecule patterning. With masks made from photoresist thin-films, researchers patterned two organosilanes on the surface of AlN through a lift-off process: APTMS (with $-NH_2$) and octadecyltrichlorosilane (OTS; with $-CH_3$).[54] Subsequently, they were able to attach antibodies on the APTMS areas and leave the OTS areas nude. Based on the phenomenon that organosilanes are degraded upon illumination with UV light, photolithography has also been applied to direct patterning of organosilanes and thus the biomolecules.[45,52] Further study revealed that the cleavage of the alkyl chain in octadecylsilane (ODS) could be achieved with UV illumination at an energy level lower than the ionization energy normally required in degradation.[57] It was speculated that this low-excitation-energy electron transfer from organosilane to the substrate material happened only in a certain energetic window defined by energy band positions of the substrate and the organosilane.[57] This UV photopatterning strategy is also applicable to other aforementioned biofunctional methods that involve UV light, such as the formation of an organophosphonic acid layer and bonding of the alkene group.[71,73,80] In the cases where biomolecules or linking molecules can be printed on III–nitrides, inkjet printing can be used to readily pattern the biomolecules.[77]

5. Biosensing mechanisms

5.1 Electrical biosensing

Electrical biosensing is the most popular signal detection mechanism of nanomaterial-based biosensors, mainly because it directly transforms the molecular phenomena into quantitative electrical signals and is suitable for data processing and storage. Electrical biosensing mechanisms of nanomaterial-based biosensors can be generally divided into two categories. One measures the change in conductance of the functional nanomaterial, induced by the presence of target markers in the proximity of the nanomaterial's surface. The other, known as electrochemical biosensing, uses electrodes decorated with nanomaterials to measure the current, potential, or impedance in an electrochemical system. Besides the common merits of high surface-area-to-volume ratios and high surface energies shared by many types of nanomaterials, the III–nitride nanomaterials possess high electron motility, surface-accumulated charge carriers, extraordinary chemical stability, and selective

interactions with specific anions, making them attractive candidates for electrical biosensors.

5.1.1 Biosensing based on conductance change. The conductance-based biosensing mechanism has been adopted by a majority of III–nitride based biosensors. The most commonly used format of signal readout is the field-effect transistor (FET), in which a III–nitride nanomaterial acts as the FET channel to connect the drain and source electrodes. The surface of the nanomaterial is usually biofunctionalized to capture specific target molecules (Fig. 4A).[81] Apparently, the configuration of the FET channel is crucial, for which one needs to select the proper material composition and surface chemical treatment of the FET channel. A short distance between the captured molecule and the location of electric phenomena occurring on the nanomaterial FET channel usually enhances the sensitivity. For example, a 2DEG in GaAlN/GaN heterostructures was employed in many conductance-based biosensors to amplify the electrical changes,[67,82–85] because the 2DEG is very sensitive to the presence of the target molecules in the proximity of the channel surface. As the first sensing applications of III–nitride nanomaterials, gas sensing used different mechanisms of conductance change. For example, dipole and redox gas molecules may affect Schottky barriers, and electric potential affects the conduction channel. Since gas sensing is not typical in biosensing, we do not discuss its detailed sensing mechanisms here. Interested readers may refer to some previous reviews.[86,87] Most biologically relevant analytes are detected in solutions, and they often accumulate or induce electrical charges on the gate area of an FET. These target molecules could affect the carrier distribution in III–nitride nanomaterials. This type of biosensor could be categorised by the charge/potential source: ion-selective FETs (ISFETs), enzyme-modified FETs (EnFETs), immunologically modified FETs (ImmunoFETs), and DNA-modified FETs (DNAFETs).

ISFETs rely on the accumulation of ions on the surface of gate area that generates electric potential to affect the carrier distributions inside nanomaterials.[88] They are often used to measure the pH of a solution. The –OH amount on the oxidized surface of III–nitride can be affected by the H^+ concentration in the solution (protonated, neutralized, or deprotonated), and this exerts a potential on the gate area. Steinhoff *et al.* have compared different III–nitride heterostructures for pH measurements and similar sensitivities were achieved from these structures.[89] It was suggested that the naturally or thermally oxidized layers of III–nitride heterostructures were responsible for the sensing performance. As for detecting other ions, InN nano-films were found to selectively respond to anions (*e.g.*, Cl^- and OH^-) rather than cations, as the positively charged surface of InN attracts and interacts with the negatively charged ions in solutions.[90] In another report, InN NF was deposited on AlGaN/GaN heterostructures as the gate area to detect Cl^-.[91] Instead of InN NF, a layer of silver/silver chloride (Ag/AgCl) electrode can be used as the gate area to detect Cl^-, because the potential of the Ag/AgCl changes with the concentration of Cl^-.[92]

EnFETs feature gate areas modified with enzymes that can react with the target molecules (*e.g.*, penicillinase and glucose oxidase). The underlying mechanism here is that the surrounding environment (*e.g.*, pH or the amount of electrons) of the gate area will be changed by the enzymatic reactions, thus affecting the electrical properties of the III–nitride nanomaterials.[93] The enzymes can be immobilized on surfaces of AlGaN/GaN heterostructures through organosilane-based

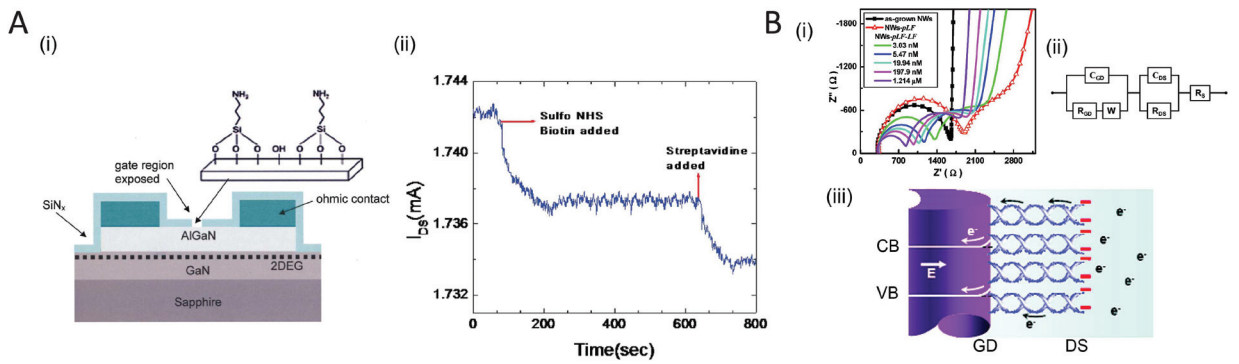

Fig. 4 Electrical biosensing mechanism. (A) Biosensor based on the change of conductance.[81] The sensor had an FET format where 2DEG was used to sense the existence of proteins (i), and the current was monitored, which showed changes due to the existence of proteins (biotin and streptavidin) (ii). Reprinted and adapted with permission from ref. 81, Copyright 2005, AIP Publishing LLC. DOI: 10.1063/1.1994951. (B) Biosensor based on the change of impedance.[101] GaN NWs were used as the transducing material, and an organosilane-based biofunctionalization process was used to immobilize probe DNA to capture the target DNA (iii). Nyquist plots demonstrated the phenomena from pristine GaN NWs, biofunctionalization and target DNA capture (i). Electrical circuits were proposed to explain the EIS results, where the introduction of DNAs added extra interfaces and consequently more target DNA capture (ii). "C_{GD}" and "C_{DS}" denote the capacitances at the GaN/DNA interface and the DNA/electrolyte interface, respectively. "R_{GD}" and "R_{DS}" denote the resistances at the GaN/DNA interface and the DNA/electrolyte interface, respectively. "R_s" denotes the resistance of the electrolyte solution. "CB" and "VB" denote the conduction band and valence band, respectively. "GD" and "DS" denote the interface between GaN NWs and DNAs, and the interface between DNAs and the electrolyte solution, respectively. Reprinted and adapted with permission from ref. 101, Copyright 2008, American Chemical Society. DOI: 10.1021/ac800986q.

chemistries, as reported in a previous study for detecting penicillin.[45] Kang *et al.* have demonstrated the possibility of selectively growing ZnO NWs on AlGaN/GaN for the sensing of glucose.[64] These one dimensional nanostructures on the gate area extend the surface area, and ZnO NWs electrostatically attract glucose oxidase for better immobilization. This method might be used in other FET sensors.

ImmunoFETs have been widely used for detecting a variety of protein biomarkers (*i.e.*, antigens and antibodies), and are based on the immunoreaction between a target biomarker and a capture probe on the surface of a III–nitride gate area. These probe molecules immobilized on the gate area bind with the specific target protein markers through immunological recognition. The target protein molecules are normally electrically charged under physiological pH conditions; thus they generate an electric potential on the gate area, affecting the conductance of the III–nitride nanomaterial underneath the gate area. A majority of the III–nitride ImmunoFETs reported so far used AlGaN/GaN heterostructures that have 2DEG layers (Fig. 4A).[62,63,81,94,95]

If the gate area of a III–nitride FET is biofunctionalized with DNAs instead of proteins, it could be used for DNA detection and thus becomes a DNAFET. In this case, single-stranded probe DNA molecules, immobilized on the surface of the gate area, bind with single-stranded target DNA molecules through hybridization. The negatively charged sugar–phosphate backbones of the target DNA molecules impose a potential on the gate area of the FET and change its conductance. AlGaN/GaN heterostructures have been used as the gate materials in previously reported DNAFETs.[83,96]

Besides the aforementioned types of FET biosensors involving III–nitride nanomaterials, there are two additional types of FET-based biosensors that are worth noting here. One is the non-enzyme detection of saccharide using AlGaN/GaN heterostructures, where the interaction of boronic acid (immobilized on the AlGaN/GaN surface) and saccharide generates an electric effect on the 2DEG of the AlGaN/GaN heterostructures.[67] The other one is the recording of cell electric activities on an AlGaN/GaN electrolyte gate FET (cell–FET), where electrogenic cells (*e.g.*, cardiac myocytes[97]) could be directly grown on the AlGaN/GaN heterostructures because of the heterostructures' good biocompatibility, and ion fluxes through the cellular membranes generate electric potentials that affect the conductance of the FET.[97]

5.1.2 Electrochemical biosensing. Unlike the FET sensors where III–nitride nanomaterials are used as the gate areas, electrochemical biosensors use III–nitride nanomaterials as the working electrodes (WEs) of electrochemical cells. Electrochemical biosensing could measure electric potential (potentiometric biosensor), current (amperometric biosensor), or impedance (impedimetric or conductrometric biosensor) as the readout signal, which is produced or affected by chemical reactions involving the target analytes. An in-depth discussion of the working principles and device architectures of existing electrochemical biosensors can be found in a recent review.[98] The main factor in electrochemical biosensor design is the configuration of the working electrode, including its material composition, size, surface morphology and treatment.

A potentiometric anion sensor that integrated a GaN thin-film WE and an Ag/AgCl reference electrode (RE) was developed in earlier reports.[99,100] The voltage between the WE and RE decreased with the concentrations of different target anions. The voltage change was induced by the interaction of the target anion and the electron-deficient Ga atoms (caused by the binding of Ga and N). The native GaN electrode showed no response to cations, but could be used in cation sensing after a cation selective membrane was deposited. InN thin films were used in a similar fashion for anion detection, taking advantage of their high surface charge densities and positively charged surface donor states.[90]

The voltammetric detection was implemented on surface-functionalized GaN NW electrodes for DNA hybridization.[50] The target DNA molecules hybridized with the DNA probe immobilized on NW surfaces, and the purine bases (*i.e.*, adenine and guanine) of the hybridized DNAs were oxidized *via* cyclic voltammetry (CV) to generate current outputs. The voltammetric DNA sensing consumes the DNAs on the electrode and is thus irreversible, and the current response only exists in the first CV scan. In contrast, impedimetric DNA detection relies on molecular biorecognition on sensing electrodes and requires relatively low voltages which do not provoke oxidation of DNA purines (Fig. 4B).[101] Chen *et al.* investigated the use of GaN NWs for electrochemical impedance spectroscopy (EIS) based detection of DNAs.[101] An equivalent circuit model was proposed to interpret the EIS measurement data (Nyquist plots), which considered both the interfaces of GaN/DNA and DNA/electrolyte (in series) and thus fit well the Nyquist data. It was found that the negatively charged DNAs, captured on the GaN NWs, marginally increased the electron transfer resistance of the DNA/electrolyte interface but significantly reduced the electron transfer resistance of the GaN/DNA interface (by flattening the surface band bending of the GaN NWs), which reduced the overall impedance between the WE and CE of the device.[101]

5.2 Mechanical biosensing

Micro and nanoscale mechanical sensing often reaches extraordinarily high resolution and is particularly suitable for measuring ultralow masses of micro- and nano-objects (*e.g.*, cells and molecules) and studying the forces or strains/stresses induced by chemical and biological molecules.[102] Existing mechanical biosensing mechanisms generally fall into quasi-static and dynamic modes. A majority of mechanical biosensors are constructed from micro and nano-beams,[103,104] while there are also surface acoustic wave (SAW) structures.[105,106] Several factors may affect the performance of mechanical biosensors, including mechanical properties and electromechanical coupling coefficients of the transducer materials. The environment could also be a crucial factor, for example, the viscosity of the surrounding fluid of the transducer structure affects damping of the dynamic sensor.

III–nitrides possess high stiffness, which leads to high sensitivity in resonant biosensors. AlN, in particular, has the merits of high stiffness, strong piezoelectric effect, high electromechanical coupling coefficient and rapid surface acoustic propagation, all beneficial to SAW biosensing.[19,20] The 2DEG in an AlGaN/GaN heterostructure is induced by both spontaneous and piezoelectric polarizations,[107] and is thus sensitive to any stress/strain applied to the heterostructure. III–nitride mechanical sensors have been developed based on mechanically-induced conductivity change of the AlGaN/AlN cantilever,[108] the AlN resonator,[109] and so forth. However, mechanical biosensing reports with III–nitride nanomaterials have been relatively rare so far. An AlN bridge resonator has been used to detect picogram mass, where the resonance was invoked by a magnetomotive mechanism.[110] Thanks to the good biocompatibility of AlN, Chinese hamster ovary (CHO-K1) cells readily adhered to the resonating beam without special surface treatment, and a drastic shift in the resonant frequency of the AlN bridge was observed upon cell adhesion (Fig. 5A).[110] In another report, it has been demonstrated that a SAW biosensor made from an AlN thin-film was capable of detecting DNAs after organosilane-based biofunctionalization (Fig. 5B).[55] An interesting study utilized the high electromechanical coupling coefficient and high propagation velocity of SAW in the AlGaN top layer of an AlGaN/GaN heterostructure, and patterned 2DEG in the AlGaN/GaN heterostructure.[111]

5.3 Optical biosensing

Optical biosensing relies on optical adsorption by accumulated target molecules on a material surface, or a change in the optical characteristics of a transducer structure due to the existence of the molecules, both of which can be quantified *via* PL and Raman spectroscopy. We will not discuss the detailed working principles of different optical biosensing mechanisms, and readers may refer to other related reviews.[112,113]

Localized surface plasmon resonance (LSPR), which typically happens at the interface of metal nanoparticles and dielectric materials or environments, generates an intense optical signal. The LSPR signal is highly sensitive to the nanoparticle composition, size, and environment, enabling LSPR-based biosensing. By depositing Ag nanoparticles on AlN nanorods (NRs), Chattopadhyay *et al.* have demonstrated surface-enhanced Raman spectrometry (SERS) based molecular sensing.[114] Another study achieved very stable and reproducible SERS detection of amino acid and bovine serum albumin (BSA) on GaN nanopillars coated with Au.[115] With III–nitride alone, Chen *et al.* demonstrated the quenching effect in the band-edge PL emission due to coverage of DNAs on GaN NWs as a sensing mechanism (Fig. 6A).[101] In another report, Wallys *et al.* showed that PL intensities of GaN and InGaN NWs changed with pH conditions (Fig. 6B), and the performance was enhanced with the application of a bias voltage.[116]

6. Biosensor fabrication

To successfully construct III–nitride nanosensors, the nanomaterial often needs to be grown or assembled on a substrate, and microfabrication techniques may also be employed to integrate the III–nitride nanomaterial with electrodes for electrical measurements. In the prevalent electrical biosensors, Ohmic or Schottky contacts between the nanomaterial and the electrodes are needed to quantify the nanomaterial's electrical response, whereas electrical passivation of the electrodes can protect them against the interference with the fluidic environment. Here we summarize existing device fabrication techniques for constructing biosensors involving III–nitride nanomaterials.

6.1 Growth and assembly of nanomaterials

Synthesis technologies for III–nitride nanomaterials have been greatly improved over the past few decades, and readers may refer to reviews dedicated to III–nitride synthesis.[10,11] Here we discuss some important issues related to biosensor construction. Growth of III–nitride nanomaterials often requires substrates with matching lattice structures and thermal properties. In existing biosensors with III–nitride nanomaterials,

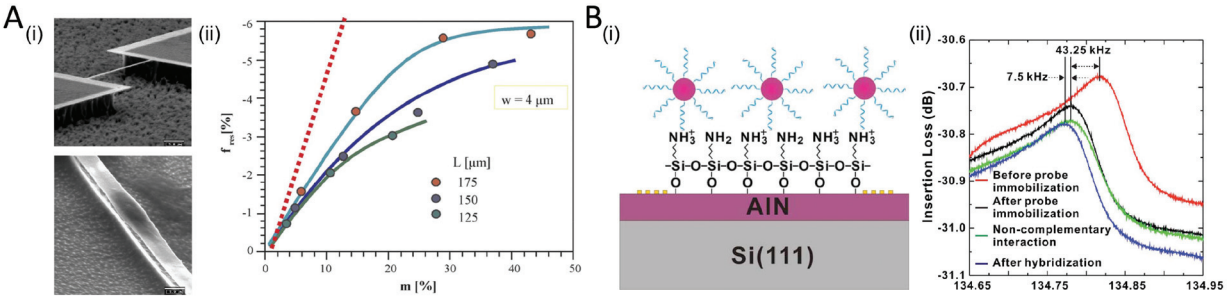

Fig. 5 Mechanical sensing mechanism. (A) Biosensor based on SAW.[148] AlN was used as the transducing material, and its surface was biofunctionalized *via* an organosilane-based process to immobilize probe DNAs (i). The resonance frequency shifts upon undergoing the biofunctionalization and target-DNA capture processes (ii). Reprinted and adapted with permission from ref. 148, Copyright 2007, Elsevier. DOI: 10.1016/j.snb.2006.10.049. (B) Biosensor based on a resonating beam.[82] CHO-K1 cells adhered to the AlN resonating beam (i). The resonance frequency of three different AlN resonating beam length configurations changed according to mass load, where the dotted line represents the theoretical expectation (ii). Reprinted and adapted with permission from ref. 82, Copyright 2008, AIP Publishing LLC. DOI: 10.1063/1.3003875.

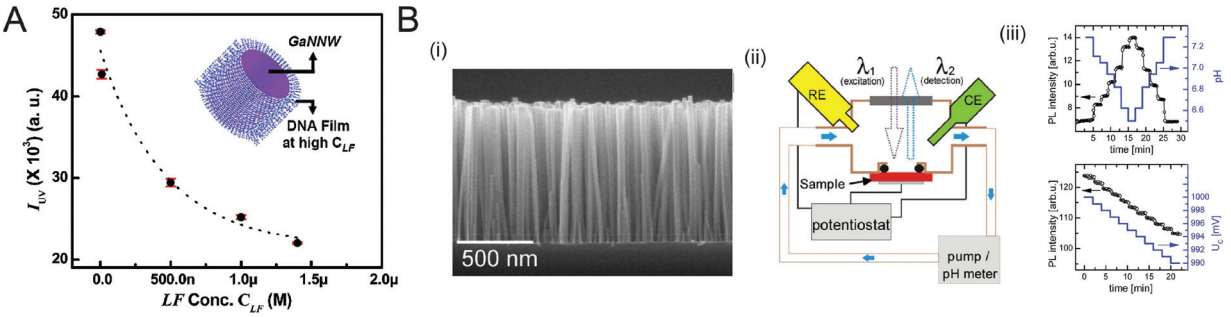

Fig. 6 Optical sensing mechanism. (A) Biosensor based on PL.[137] The UV intensity of the GaN-NW biosensor changed with the target DNA concentration. Reprinted and adapted with permission from ref. 137, Copyright 2008, American Chemical Society. DOI: 10.1021/ac800986q. (B) Biosensor based on PL under biased voltage.[154] Well-aligned GaN NWs were used as the transducing material (i). The characterization setup included both electrochemical and optical systems (ii). The PL intensity changed with varied pH values of phosphate buffered saline solution (top) and changed with varied cathodic bias at pH 7.05 (bottom) (iii). Reprinted and adapted with permission from ref. 154, Copyright 2012, American Chemical Society. DOI: 10.1021/nl303021v.

the most commonly used substrate is silicon wafer.[55,117,118] Sapphire (Al_2O_3) is another popular choice as the device substrate, which is transparent and stable at high temperature.[89,119,120] But it has unsatisfactory thermal and structural matching with III–nitrides. On the top of the substrate, a buffering layer (*e.g.*, AlN) is sometimes necessary before growing the transducer material, in order to obtain a particular polarity or better growth quality.[121,122] For the assembly of NWs, two strategies have been developed. One is assembly after growth, which requires the transfer of NWs from a growth substrate to a device substrate. This kind of assembly techniques for NWs including III–nitrides typically utilize a fluid flow,[123] an electric field,[124,125] a mechanical shear force,[126] and so forth (Fig. 7A).[127,128] The second strategy is *in-situ* guided growth, which utilizes the crystal and the graphoepitaxial effect on the surface of growth substrates (Fig. 7B).[129,130] It allows horizontal growth of NWs on a device substrate, and avoids the transfer process. An assembled array of NWs, combined with microfluidic channels (for solution delivery), can achieve high efficiency in multiplexed biosensing.[131]

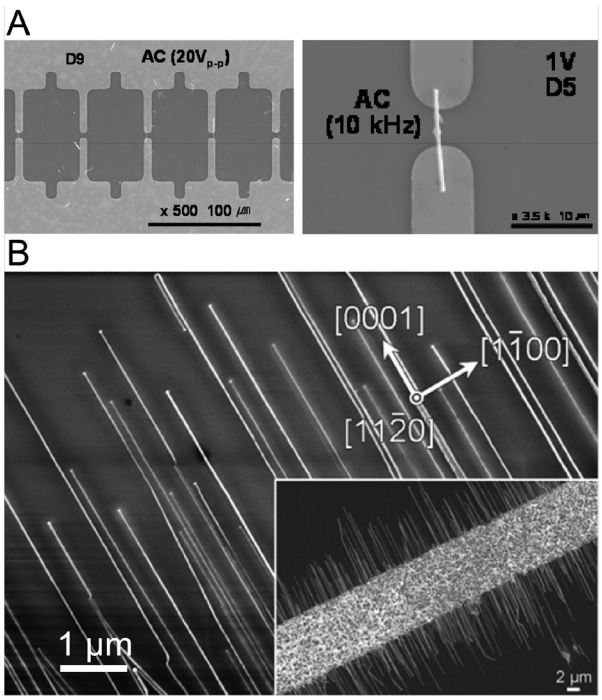

Fig. 7 Lateral alignment of NWs. (A) Assembly of Ga NWs on microfabricated electrodes *via* dielectrophoretic alignment under alternating current.[164] Reprinted and adapted with permission from ref. 164, Copyright 2006, IOP Publishing. DOI: 10.1088/0957-4484/17/14/009. (B) Laterally aligned GaN NWs obtained by guided growth on quartz.[169] Reprinted and adapted with permission from ref. 169, Copyright 2014, American Chemical Society. DOI: 10.1021/nn4066523.

6.2 Microfabrication of nanomaterials

Microfabrication for selective material removal (*e.g.*, etching) is sometimes needed, mostly for patterning III–nitride nano-films. Because of their extraordinary chemical stability, conventional wet etching, often, cannot effectively remove III–nitrides. The effective etching technologies for the wide bandgap semiconductor materials including III–nitrides are mainly plasma-based dry etching, such as reactive ion etching, electron cyclotron resonance, and inductively coupled plasma etching.[132] In order to form free-standing III–nitrides, two strategies are optional. One is to selectively etch the III–nitrides and the substrate materials together after growth, and the other one is to selectively pattern the substrate with conventional micromachining before growth of III–nitrides on them, which allows selective growth of III–nitrides.[109] The latter one is comparatively convenient. Upon designing a microfabrication process, one should note that the process might induce some modification in the properties of III–nitride nanomaterials. Readers may refer to previous studies on the impact of the fabrication process on surface properties, electrical performance and biocompatibility.[40,133]

6.3 Electrical contact and passivation

Ti/Al/Ni/Au is a widely used combination of electrode materials for building Ohmic contacts with III–nitrides. Thin

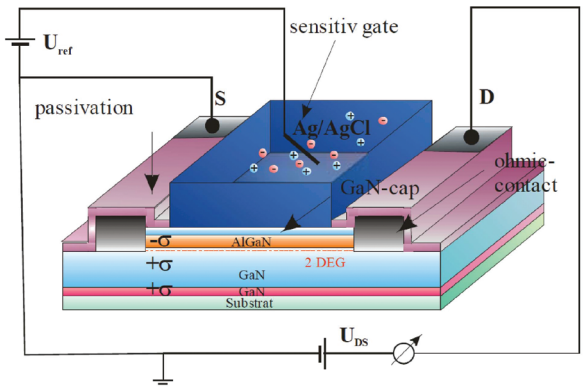

Fig. 8 Schematic of the electrical contact and passivation layout on III–nitride nanobiosensors.[130] "S" denotes source, and "D" denotes drain. Reprinted and adapted with permission from ref. 130, Copyright 2010, John Wiley and Sons. DOI: 10.1002/pssc.200983531.

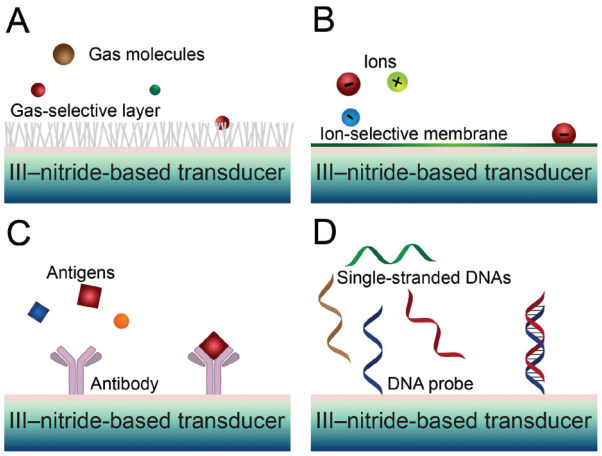

Fig. 9 Typical biosensing molecules targeted by III–nitride nanobiosensors. Gases (A), ions (B), proteins (C), and DNAs (D) are detected as biosensing targets through their own specific recognition systems.

films of Ti/Al/Ni/Au are usually deposited sequentially through electron-beam evaporation and then thermally annealed.[49,134] Other similar electrode compositions that generate Ohmic contact with III–nitrides include Ti/Au,[135] Ti/Al/Mo/Au,[136] and Ti/Al/Pt/Au.[81] Deposition of some metals (*e.g.*, Pt[137] and Pd[138]) could form Schottky contact, as we mentioned in the section on electrical biosensing. In most biosensing applications, the device needs to handle fluids, and it is mandatory to ensure that only the transducer III–nitride nanomaterial contacts the fluids while the electrodes are protected from the fluids by an insulating layer (passivation). This will guarantee that the electrical signal induced by the molecular sensing process would not be disturbed by the fluid-induced noises (from the electrodes), and that the electrodes would not be damaged by the fluid. The passivation can be achieved by coating the electrodes with a thin film of Si_3N_4 [81] or polymethyl methacrylate (PMMA).[62,64] A schematic of the typical contact and passivation layout on III–nitride nanobiosensors is shown in Fig. 8.[96]

7. Biosensing applications

Detection of gases, ions, proteins and DNAs cover a vast majority of applications of III–nitride nanobiosensors. To ensure the specificity and sensitivity, the detection of a specific category of target molecules utilizes a corresponding recognition system: a gas-selective layer for gas sensing; an ion-selective membrane for ion sensing; antibody–antigen immunorecognition for protein sensing; and DNA hybridization for DNA sensing (Fig. 9). In this section, we describe the typical biosensing targets, the corresponding III–nitride nanobiosensors reported so far, and the important design considerations of biosensors for specific targets. The key information on the biosensing targets and the performance of the reported III–nitride nanobiosensors is summarised in Table 1.

7.1 Gases

The first major category of molecular sensing with III–nitride nanomaterials is gas sensing. Some gases (*e.g.*, H_2) are less biologically or clinically relevant, while some others are important physiological markers such as carbon monoxide (CO), carbon peroxide (CO_2) and oxygen (O_2).

CO is a common toxic molecule and causes cellular asphyxia at high concentrations, but it also confers cytoprotection at low concentrations during ischemia/reperfusion or inflammation-induced tissue injury.[139] In the report by Lo *et al.*, ZnO NRs were grown on the gate area of the GaAlN/GaN heterostructure, and CO was detected with increased sensitivity at high temperature.[140] The working principle of this sensor is that CO comes to react with O_2 absorbed on ZnO-NR surfaces to generate CO_2. The electrons formerly captured by O_2 are set free to generate a larger negative potential, which counters the 2DEG in the GaAlN/GaN hetetrostructure. In a later study, ZnO NWs were coated on the AlGaN/GaN heterostructure for CO detection utilizing a similar working principle.[141,142] These reported sensors responded to the presence of CO at room temperature, while conventional III–nitride gas sensors in a diode format typically require high temperature. So these sensors may have better potential in real-world biomedical applications.

The detection of CO_2 is also relevant to biological and medical applications, because its concentration in the patient's exhaled air is an important index in ventilation and circulation monitoring. In addition, CO_2 sensing is necessary in cell culture incubators or bioreactors to regulate the pH level of culture medium. Polyethyleneimine (PEI)/starch was spin-coated on the gate of the AlGaN/GaN heterostructure, as a specific carbon dioxide recognition layer.[143] The function of the sensor relies on the reaction between the amino group of PEI and CO_2 with water and starch, which generates $OCOOH^-$ ions affecting the surface electric potential of the AlGaN/GaN

Table 1 Biosensing applications of III–nitride nanomaterials

Category	Target	Device structure	Sensing mechanism	Surface functionalization	LOD	Sensitivity	Ref.
Gas	H_2, HC, CO, NO	FET: AlGaN/GaN heterostructure with a GaN layer as the cap and Pt as the gate on the cap	Electrical: GaN/Pt Schottky barrier height changes upon gas introduction, and the AlGaN/GaN heterostructure amplifies the signal.				165
	H_2, CO, C_2H_2, NO_2						121
	H2, HC, CO, NO_x						166
	O_2	FET: AlGaN/GaN with a InZnO layer as the gate	Electrical: Because of oxygen vacancy, the conductance of InZnO changes with partial pressure of oxygen, and the AlGaN/GaN heterostructure amplifies the signal.				144
	CO	FET: AlGaN/GaN with ZnO NWs/NRs grown on the gate area	Electrical: CO is absorbed on the ZnO NW surface and releases more electrons as counter charges that affect the 2DEG in the AlGaN/GaN heterostructure.		100 ppm at 25 °C and up to 30 ppm at 150 °C	$\Delta I/I$ is 0.23% at 25 °C and 7.5% at 150 °C.	140
	CO				400 ppm with polar ZnO NWs, and 3200 pm with nonpolar ZnO NWs		141
	CO_2	FET: AlGaN/GaN heterostructure	Electrical: The amino groups of PEI interact with CO_2 and generate charges which affect the 2DEG of the AlGaN/GaN heterostructure.	PEI and starch			143
Ion	pH	FET: GaN:Si/GaN:Mg heterostructure	Electrical: There are –OH groups on the oxidized surfaces, and the groups can be affected by the H^+ concentration in the solution (protonated, neutralized, or deprotonated), exerting voltage on the gate area.	Native oxide	0.1 pH	57.3 mV pH^{-1}	89
				Thermal oxide	0.1 pH	56.6 mV pH^{-1}	
		FET: AlGaN/GaN heterostructure with GaN as the cap		Native oxide	0.05 pH	56.0 mV pH^{-1}	
		FET: AlGaN/GaN heterostructure		Native oxide	0.4 pH	70 μA pH^{-1} at source–drain bias of 0.25 V	117
				UV-ozone-induced oxide	0.2 pH	37 μA pH^{-1} at source–drain bias of 0.25 V	
				Sc_2O_3 deposited	0.1 pH	37 μA pH^{-1} at source–drain bias of 0.25 V	
		FET: AlN/GaN heterostructure with GaN as the cap and a 2DEG-to-surface distance down to 7.5 nm			0.005 pH	52 mV pH^{-1}; 6.6 μA pH^{-1} under gate–drain voltage of −0.24 V	146
		GaN or InGaN NWs	Optical: The position of the band edges of NWs changes with the redox level of analytes, reflected in PL of NWs. Surface recombination between NWs and analytes can be suppressed by bias voltage, which boosts the sensitivity.		0.05 pH		116

Table 1 *(Contd.)*

Category	Target	Device structure	Sensing mechanism	Surface functionalization	LOD	Sensitivity	Ref.
	Cl^-	FET: AlGaN/GaN heterostructure with AgCl/Ag/Pt on the gate area	Electrical: The potential of AgCl/Ag electrode changes with Cl^- concentration which exert on the 2DEG of the AlGaN/GaN heterostructure.		1×10^{-8} M with a 20×50 μm^2 gate area		92
		FET: InN/AlN layer where InN is as thin as 10 nm	Electrical: The positively charged surface states on InN surfaces selectively adsorb anions, generating voltage that affects the carrier distribution.		0.25 *p*Cl (*p*Cl denotes −log [Cl^-])	5 μA *p*Cl^{-1}	147
		FET: AlGaN/GaN heterostructure with InN on the gate area					91
	SCN^-, $C_7H_5O_3^-$, I^-, ClO_4^-, NO_3^-, Br^-, CH_3COO^-, Cl^-, F^-	Electrochemical cell: GaN film as the working electrode	Electrical: Selective interaction of the electron-defective Ga atoms with the anions generates potential and affect impedance.				99
	Cl^-, HPO_4^{-2}, ClO_4^-, K^+, pH						100
	Cl^-, OH^-	Electrochemical cell: InN film as the working electrode	Electrical: The positively charged surface states on InN surfaces selectively adsorb anions which generates potential.			47 mV per decade for Cl^-, −45 mV per decade for Cl_2^{-2}, −49 mV decade for OH^-	90
Protein	Streptavidin	FET: AlGaN/GaN heterostructure	Electrical: Immunological binding between antibody and target antigen which has charges under sensing condition and the charges affect the 2DEG of the AlGaN/GaN heterostructure.	Organosilane-based functionalization, terminating with corresponding probe molecules.			81
	Prostate specific antigen				4.73 pM		116
					<0.1 pg ml^{-1}		148
	Kidney injury molecule-1			Gold or gold alloy deposited on the gate area, terminating with the specific antibody or other types of protein through a series of biofunctionalization	10 pg ml^{-1}		62
	C-erbB-2				1 ng ml^{-1}		64
	Botulinum toxin				0.25 μg ml^{-1}		63
	Efavirenz				1 ng ml^{-1}		150
	Peptide				0.021 nM		152
	Perkinsus marinus				10 pM		85
	Vitellogenin						66
	C-reactive protein (CRP)				2 μg ml^{-1}		95
					4 μg ml^{-1}		151
	SRC kinase				0.1 ng ml^{-1}		149
					1 pM		167

Table 1 *(Contd.)*

Category	Target	Device structure	Sensing mechanism	Surface functionalization	LOD	Sensitivity	Ref.
DNA	Single-stranded DNA			Gold-coated gate area, terminating with thiol-modified strand probe DNA			168
		FET: Commercial FET using GaN NWs as the extended gate		Organosilane-based functionalization, terminating with thiol-modified DNA	10^{-18} M		118
		Electrochemical cell: GaN NWs are used as the working electrode	Electrical: The probe DNA strand captures the target DNA strand which changes the surface electron transfer resistance reflected in impedance on the working electrode.		10^{-19} M		155
		GaN NWs.	Optical: The probe DNA strand captures the target DNA strand which reduces available radiative density on NWs and quenches PL.				101
		AlN film	Mechanical: The probe DNA strand captures the target DNA strand which changes the resonance frequency when SAW propagates on NF.	Organosilane-based functionalization, terminating with gold nanoparticle surounded by thiol-modified DNA		15 Hz cm^2 ng^{-1}	55
Cell	Action potential of cardiac myocyte cell	FET: AlGaN/GaN heterostructure	Electrical: Electrical signals generated by cellular actions affect the carrier distribution of the nanomaterials.				97
	Ion channel activity						158
							157
	Acetylcholine (ACh)			Gate area is modified by acetylcholinesterase			159
	Behaviors of *Physarum* cells		Impedance is measured on the gate area				160
	CHO-K1 cell	Beam: AlGaN/GaN heterostructure	Mechanical: Cellular mass changes the resonator frequency of the beam, where the resonance is magnetomotively or piezoelectrically activated.				169
		Beam: AlN film					110
Other	pH and glucose	FET: AlGaN/GaN heterostructure	Electrical: pH level changes hydroxyl groups on the oxide and glucose oxidation generates charges, both of which affect the 2DEG in the AlGaN/GaN heterostructure.	Sc_2O_3 gate for pH sensing, and ZnO NWs immobilized with GOx on the gate area for glucose sensing.			82
	Fructose, galactose and glucose		Electrical: Saccharide molecules affect the 2DEG in the AlGaN/GaN heterostructure.	Gold-coated gate, terminating with thiol-modified boronic acid.			170

heterostructure. However, the sensor was tested at temperatures from 46 to 220 °C, which might constrain its biomedical applications.

O_2 has been detected with an InZnO film, and the AlGaN/GaN structure was arranged underneath the InZnO film to amplify the sensing signal.[144] The source–drain current of the sensor decreases in O_2 ambience, because the O_2 molecule comes to react with oxygen vacancies of the InZnO film, causing a potential change that affects the AlGaN/GaN heterostructure. The sensor showed no response at room temperature, and generated high-quality sensing signals at the temperature of 120 °C.[144] Lopez-Gejo reported oxygen sensing achieved with luminescent Ru(II) complexes bonded on p-GaN, based on the optical sensing mechanism.[46,56] Its function relies on the quenching effect of the oxygen molecule on the Ru(II) complex luminescence. GaN was used not only as a substrate but also as an excitation source, reducing the sensor structure size.

7.2 Ions

Ion sensing forms a big part of biosensing, because the ionic environment greatly affects biological activities, ionic concentrations can be used as indicators for biological activities, and the ion sensing principles can be leveraged for detection of other markers.[88] ISFET is arguably the most popular type of ion sensor mentioned above. In order to improve the sensing performance in ion detection, one may refer to the model proposed by Podolska *et al.*, which has been validated through experiments.[145]

A basic type of ion sensing is pH detection. Conventional glass electrodes are widely used for pH sensing, but are fragile and need calibration before use as their characteristics drift after long-time use. III–nitrides, in contrast, are mechanically, thermally and chemically stable, and are therefore excellent substitutes for glass electrodes. According to the reports on III–nitride-based pH sensing where different sensor formats were utilized, specific sensing mechanisms were proposed. One needs to understand the sensing mechanism before improving the sensor performance. In typical ISFETs, pH sensing performance has been found to be associated with the gate oxide layer. Kang *et al.* compared different gate oxides, and Sc_2O_3 layers deposited by molecular beam epitaxy (MBE) were found to give high pH sensing resolution.[117] Another improvement in ISFET was accomplished using an ultrathin barrier layer in the AlN/GaN heterostructure with 2DEG, which generated not only higher transconductance (reflected by high source–drain current change), but also a smaller shift of gate–drain voltage from zero. This means that this design could provide good sensitivity without requiring an RE.[146] In electrochemical pH sensors, the electrical response to pH relies on the interaction between OH^- and GaN or InN, and the positively charged surface state of InN could generate a higher response.[90,100] As for optical pH sensing using GaN and InGaN NWs, the pH condition regulates the PL intensity of the III–nitride NWs. The PL intensity decreases with the pH-induced surface recombination and hole transfer from NWs, and it was found that the device sensitivity could be further improved by applying a proper external bias voltage.[116]

The detection of a wide range of other ions has also been demonstrated with either ISFETs or electrochemical sensors based on III–nitride materials, which rely on different working principles to ensure their selectivity. In ISFETs for Cl^- sensing, Hung *et al.* formed an Ag/AgCl layer through potentiostatic anodization on the gate area of the AlGaN/GaN heterostructure, and the electric potential of this layer was altered due to the existence of Cl^- ions. Furthermore, this potential change affected the charge density inside the AlGaN/GaN heterostructure.[92] InN NFs were also used in more than one sensor design for anion sensing. The positive surface charge donors of the InN NF can selectively absorb anions from solution, which affects the electron distribution inside the NF. The InN NFs were grown on an AlN buffer layer,[147] or an AlGaN/GaN heterostructure for Cl^- detection,[91] with which researchers found cations had no impact on the detection. In the electrochemical ion sensor using III–nitrides, it was also found that only anions selectively interact with electron-defective Ga atoms[99,100] or the surface states on InN,[90] and an ion selective membrane may thus be needed to detect cations.[100]

7.3 Proteins

Proteins are essential building blocks of living organisms, representing a paramount type of biomarkers in biological research and disease diagnostics. Most protein biosensors rely on the immunological recognition between antibody and antigen proteins, as introduced in section 5. The sensors made from III–nitride nanomaterials can generate electrical output signals in response to the presence of target protein markers on the surface of the III-nitride nanomaterials. They do not need any label (*e.g.*, fluorescence tags in fluorescence biosensing, or enzymes and substrates in ELISAs), and thus allow label-free biosensing. A very important factor that affects the biosensing performance is the biofunctionalization of the transducer material. High coverage of probe proteins on the sensor assures high capture efficiency, and proper chemical linkage between the nanomaterial surface and the probe molecules also facilitates the attainment of high accuracy and sensitivity (as discussed in section 4.2).

Most of the existing protein sensors with III–nitride nanomaterials utilize the configuration of AlGaN/GaN heterostructure ImmunoFETs, where electric current, conductance or resistance is monitored as the signal output. Kang *et al.* demonstrated one of the first protein sensors with III–nitride FET, where a decrease in the current of the ImmunoFET was observed after the addition of biotin and the capture of streptavidin in the sensing process.[81] Later, the protein targets measured by III–nitride ImmunoFETs expanded to a variety of applications. Most of the protein targets were associated with specific diseases, including prostate specific antigen (PSA) as the marker for prostate cancers,[62,148] kidney injury molecule-1 for early kidney injury detection,[64] c-erbB-2 as a breast cancer marker,[63] and more recently, C-reactive protein that reflects inflammatory conditions.[149] Besides applications in disease

diagnosis, ImmunoFETs were also used to detect botulinum toxin—a marker for biological weapons,[150] and *Perkinsus marinus*—a protozoan pathogen that causes widespread mortality in oyster populations.[66] For environmental safety, vitellogenin as an endocrine disrupter biomarker was measured.[95,151] In several recent reports, III–nitride ImmunoFETs were used in biochemical and pharmaceutical studies to analyze the binding affinity between anti-ferritin heavy-chain antibody and a peptide,[85] investigate the binding sites between human immunodeficiency virus reverse transcriptase (HIV-RT) and its inhibitor efavirenz,[152] and quantify kinase amount for understanding the kinome activity.[153]

From a practical point of view, the LOD is an important parameter of biosensing performance. Li *et al.* were able to detect PSA with an LOD down to 0.1 pg ml^{-1}, the smallest one reported so far.[154] In comparison with a previous III–nitride ImmunoFET for PSA in which gold was deposited on the gate region for biofunctionalization,[62] the lower LOD in the report by Li *et al.* might be a result of the smaller distance between biomolecules and 2DEG. Another important feature of FET sensors is a rapid response that allows real-time monitoring of protein binding, and many of the III–nitride ImmunoFETs were able to respond within 5 s and thus work in a real-time fashion.[62,66,94]

7.4 DNAs

DNAs carry genetic information that regulates the development and physiology of living organic systems. DNA sensing mostly relies on the hybridization of matched DNA strands to achieve specificity, for which probe DNA strands are immobilized on the nanomaterial surface through biofunctionalization. Particular DNA sequences can be associated with biological or medical purposes. For example, Sahoo *et al.* detected the sequence adopted from H1N1 Swine flu gene,[155] and Chen detected the sequence corresponding to human p53 tumor-suppressor gene.[101]

III–nitride nanomaterials have also been used for label-free detection of DNAs, and the reports on DNA sensing using III–nitrides employed quite distinct working principles. DNA sensing can be conducted with an AlGaN/GaN heterostructure FET,[83] as the target DNAs bring negative charges to the nanostructure surface. An interesting study connected the gate area of a commercial FET to the GaN NWs which were functionalized with probe DNA strands, and the charge rearrangement on the GaN NWs, caused by the hybridization of DNAs, changed the bias voltage on the gate.[118] This sensor design generates ultra-high sensitivity, and is easy to assemble and handle compared with single-NW devices. DNA sensing can also be performed *via* electrochemical mechanisms, such as amperometric and impedimetric measurements.[50,101] The latter is more desirable as it does not consume the analyte. In addition, optical sensing with GaN NWs (through PL measurements) and mechanical SAW with AlN nano-film were also developed for DNA detection.[55,101]

With regard to sensing performance, Espinosa *et al.* reached an LOD of 10^{-14} M using the popular AlGaN/GaN heterostructure.[156] More importantly, they carried out a theoretical investigation to understand the sensing performance. Chen *et al.* reported an ultralow LOD down to 10^{-18} M in the FET format.[118] More recently, Sahoo *et al.* achieved an LOD as low as 10^{-19} M,[155] where the ultrasensitivity was partially due to the impedimetric sensing mechanism.

7.5 Cells

Cells are the basic unit of living organisms, and their activities involve many kinds of fascinating phenomena. As mentioned before, some III–nitrides have very good biocompatibility, making it possible to directly grow and monitor cells on devices. The reports published so far typically utilized the AlGaN/GaN heterostructures with cells directly grown on the gate area.

Steinhoff *et al.* monitored extracellular action potentials from a confluent layer of rat heart muscle cells directly cultured on a FET consisting of AlGaN/GaN, yielding a high signal-to-noise ratio.[97] Later studies recorded the activity of cells in response to chemical environment changes like calcium and inhibitor.[157,158] Beyond simple electrical signals of cell activity, AlGaN/GaN FET was also used to detect the release of acetylcholine from neuronal tissue.[159] Witte *et al.* demonstrated that high-frequency impedance measurements at the interface between the FET gate area and the cultivated cells can be used to analyse both static and dynamic characteristics of the cells.[160]

7.6 Others

Enzymes, which are proteins, are used in III–nitride biosensors for the detection of metabolic markers (*e.g.*, glucose and uric acid), and the origin of electrical signal in the enzymatic reactions is often the change of pH in the gate area of the nanomaterials.[45,161] In a report, ZnO NRs were grown on the gate area of the AlGaN/GaN heterostructure for enzymatic glucose sensing.[64] ZnO NRs are particularly suitable for immobilizing the enzyme for glucose sensing (glucose oxidase), because their surface charge state allows them to easily immobilize the glucose oxidase *via* electrostatic absorption. In another report, both physisorption and covalent bonding with organosilane were employed to immobilize penicillinase, and the covalent bonding was found to give more reproducible performance in the detection of penicillin G.[45] Apart from enzymatic sensing, fructose, galactose and glucose were detected using boronic acid receptor with a thiol-modified terminal.[67]

7.7 Driving III–nitride nanobiosensors toward real applications

Many previous studies on developing III–nitride nanobiosensors have focused on proof-of-concept demonstrations, but few of them has demonstrated the use of these promising prototypes in real-world applications. Here, we highlight some reports that have come closer to the practical uses of III–nitride nanobiosensors, in the hope that these designs may enlighten future efforts to push III–nitride nanobiosensors to the real world. Besides, for real applications, it is preferred that the sensors can directly detect molecules from untreated

or less treated biological samples, and Chu *et al.* have validated their III–nitride sensor in largemouth bass serum samples.[95] In a previous report, researchers connected silicon wafer grown with GaN NWs to a commercial FET.[157] The use of NW networks instead of single NWs and the design of connecting the GaN-NW network to a commercial FET significantly simplified the device assembly, and meanwhile, maintained its high sensitivity. In another report, glucose and pH detection in exhaled breath condensate was realized using the AlGaN/GaN heterostructure, and the biosensor was integrated on a wireless data transmission system.[82] The real-time detection of both glucose and pH using this biosensor allowed closer awareness of the glucose condition, because the glucose oxidizer's performance is affected by the pH level. The integration with a wireless system also enabled remote monitoring. There is a growing trend of using cell-phone-based diagnosis in telemedicine,[162,163] and GaN-film-based LEDs show the capability to act as microscale portable emission sources for luminescent oxygen indicators,[46,56] which may be extended to other cell-phone-based optical sensors. When the biosensor is activated, a cell-phone camera can be used to capture the image, and the colorimetric output of the biosensor can be analyzed by a phone application or sent to physicians for remote analysis. To make the sensor portable and stable against varied conditions (*e.g.*, light and temperature), Lee *et al.* have utilized a small Pt quasi-reference electrode and integrated a non-functionalized reference sensor in a III–nitride ImmunoFET.[149]

8. Closing remarks

III–nitride nanomaterials hold great promise for biosensing because of their preferable characteristics such as high chemical stability, biocompatibility, high surface carrier accumulation, and unique electromechanical properties. The substantial improvement of their growth and fabrication techniques has allowed in-depth research of their applications in biosensing. A variety of surface functionalization approaches and biosensing mechanisms have been explored, demonstrating their excellent performance including high accuracy, sensitivity and specificity. Previous research has established a solid foundation for future development of III–nitride nanobiosensors, with the eventual goal of utilizing these devices in practical applications and making a real impact on society. We anticipate that, with the further technological advancements in the field, more and more III–nitride nanobiosensors will be developed to provide higher biosensing performance, higher reliability, and better user-friendliness.

In the further development of more exciting III–nitride biosensing technologies, we envision the following directions to be explored. First, III–nitride nanomaterials still require relatively sophisticated processes for material growth and unconventional techniques for device fabrication. Future explorations of their potential in biosensing will benefit from the lowering of these technological barriers. Second, existing biosensing applications of the III–nitride nanomaterials mostly rely on electrical mechanisms, while their excellent mechanical and optical properties have not been fully leveraged. So the mechanical and optical mechanisms are worth more research efforts. Furthermore, III–nitrides will allow simultaneous multi-parameter detection in different mechanisms as shown in the reports mentioned above. Last, other important applications of III–nitrides can be integrated with biosensors. For example, III–nitrides have been studied for light emission for a long time, which might be employed in biosensing. They can also be used as a photodetector, and the bandgap can be tuned for specific detection purposes.[164]

Acknowledgements

We acknowledge financial support from the Natural Sciences and Engineering Research Council of Canada (NSERC) (Grant No. RGPIN 418553-12 and STPGP 463182-14), the Canada Research Chairs Program (Grant No. 237293), the McGill Chwang-Seto Faculty Scholarship Program (Grant No. 234304; to X. Liu), and the NSERC-CREATE Training Program in Integrated Sensor Systems (to X. Li).

References

1 A. P. F. Turner, *Chem. Soc. Rev.*, 2013, **42**, 3184–3196.
2 F. J. Gruhl, B. E. Rapp and K. Lange, *Adv. Biochem. Eng./Biotechnol.*, 2012, **133**, 115–148.
3 J. Kirsch, C. Siltanen, Q. Zhou, A. Revzin and A. Simonian, *Chem. Soc. Rev.*, 2013, **42**, 8733–8768.
4 X. Ceto, N. H. Voelcker and B. Prieto-Simon, *Biosens. Bioelectron.*, 2016, **79**, 608–626.
5 Y. Cui, Q. Q. Wei, H. K. Park and C. M. Lieber, *Science*, 2001, **293**, 1289–1292.
6 K. Balasubramanian and M. Burghard, *Anal. Bioanal. Chem.*, 2006, **385**, 452–468.
7 F. Patolsky, G. Zheng and C. M. Lieber, *Nanomedicine*, 2006, **1**, 51–65.
8 O. N. Oliveira, R. M. Iost, J. R. Siqueira, F. N. Crespilho and L. Caseli, *ACS Appl. Mater. Interfaces*, 2014, **6**, 14745–14766.
9 W. Lu and C. M. Lieber, *J Phys. D: Appl. Phys.*, 2006, **39**, R387–R406.
10 X. Wang and A. Yoshikawa, *Prog. Cryst. Growth Charact.*, 2004, **48–49**, 42–103.
11 O. Ambacher, *J Phys. D: Appl. Phys.*, 1998, **31**, 2653–2710.
12 S. J. Pearton, B. S. Kang, B. P. Gila, D. P. Norton, O. Kryliouk, F. Ren, Y. W. He, C. Y. Chang, G. C. Chi, W. M. Wang and L. C. Chen, *J. Nanosci. Nanotechnol.*, 2008, **8**, 99–110.
13 S. Chattopadhyay, A. Ganguly, K.-H. Chen and L.-C. Chen, *Crit. Rev. Solid State*, 2009, **34**, 224–279.
14 R. Kirste, N. Rohrbaugh, I. Bryan, Z. Bryan, R. Collazo and A. Ivanisevic, *Annu. Rev. Anal. Chem.*, 2015, **8**, 149–169.

15 T. Hanada, in *Oxide and Nitride Semiconductors*, ed. T. Yao and S.-K. Hong, Springer, Berlin, Heidelberg, 2009, ch. 1, vol. 12, pp. 1–19.
16 J. Q. Wu, *J. Appl. Phys.*, 2009, **106**, 011101.
17 T. Saito, T. Hitora, H. Hitora, H. Kawai, I. Saito and E. Yamaguchi, *Phys. Status Solidi C*, 2009, **6**, S658–S661.
18 J. L. Pau, J. Anduaga, C. Rivera, A. Navarro, I. Alava, M. Redondo and E. Munoz, *Appl. Opt.*, 2006, **45**, 7498–7503.
19 S. Tadigadapa and K. Mateti, *Meas. Sci. Technol.*, 2009, **20**, 092001.
20 Y. Takagaki, P. V. Santos, E. Wiebicke, O. Brandt, H. P. Schonherr and K. H. Ploog, *Appl. Phys. Lett.*, 2002, **81**, 2538–2540.
21 H. Lu, W. J. Schaff, L. F. Eastman and C. E. Stutz, *Appl. Phys. Lett.*, 2003, **82**, 1736–1738.
22 H. Lu, W. J. Schaff and L. F. Eastman, *J. Appl. Phys.*, 2004, **96**, 3577–3579.
23 T. H. Young and C. R. Chen, *Biomaterials*, 2006, **27**, 3361–3367.
24 M. Hofstetter, J. Howgate, M. Schmid, S. Schoell, M. Sachsenhauser, D. Adiguzel, M. Stutzmann, I. D. Sharp and S. Thalhammer, *Biochem. Biophys. Res. Commun.*, 2012, **424**, 348–253.
25 P. Sahoo, P. S. Murthy, S. Dhara, V. P. Venugopalan, A. Das and A. K. Tyagi, *J. Nanopart. Res.*, 2013, **15**, 1841.
26 D. Krewski, R. A. Yokel, E. Nieboer, D. Borchelt, J. Cohen, J. Harry, S. Kacew, J. Lindsay, A. M. Mahfouz and V. Rondeau, *J. Toxicol. Environ. Health, Part B*, 2007, **10**, 1–269.
27 S. Verstraeten, L. Aimo and P. Oteiza, *Arch. Toxicol.*, 2008, **82**, 789–802.
28 G. Steinhoff, O. Purrucker, M. Tanaka, M. Stutzmann and M. Eickhoff, *Adv. Funct. Mater.*, 2003, **13**, 841–846.
29 A. Podolska, S. Tham, R. D. Hart, R. M. Seeber, M. Kocan, M. Kocan, U. K. Mishra, K. D. G. Pfleger, G. Parish and B. D. Nener, *Sens. Actuators, B*, 2012, **169**, 401–406.
30 D. Kim and A. E. Herr, *Biomicrofluidics*, 2013, **7**, 41501.
31 F. Xia and L. Jiang, *Adv. Mater.*, 2008, **20**, 2842–2858.
32 C. Buchheim, G. Kittler, V. Cimalla, V. Lebedev, M. Fischer, S. Krischok, V. Yanev, M. Himmerlich, G. Ecke, J. A. Schaefer and O. Ambacher, *IEEE Sens. J.*, 2006, **6**, 881–886.
33 I. Dziecielewski, J. L. Weyher and W. Dzwolak, *Appl. Phys. Lett.*, 2013, **102**, 043704.
34 J. Y. Li, Q. S. Han, X. H. Wang, R. Yang and C. Wang, *Colloids Surf., B*, 2014, **123**, 293–301.
35 S. A. Jewett, M. S. Makowski, B. Andrews, M. J. Manfra and A. Ivanisevic, *Acta Biomater.*, 2012, **8**, 728–733.
36 C. M. Foster, R. Collazo, Z. Sitar and A. Ivanisevic, *Langmuir*, 2013, **29**, 8377–8384.
37 L. E. Bain, R. Collazo, S. H. Hsu, N. P. Latham, M. J. Manfra and A. Ivanisevic, *Acta Biomater.*, 2014, **10**, 2455–2462.
38 J. Li, Q. Han, X. Wang, R. Yang and C. Wang, *Colloids Surf., B*, 2014, **123**, 293–301.
39 J. Li, Q. Han, Y. Zhang, W. Zhang, M. Dong, F. Besenbacher, R. Yang and C. Wang, *ACS Appl. Mater. Interfaces*, 2013, **5**, 9816–9822.
40 I. Cimalla, F. Will, K. Tonisch, M. Niebelschütz, V. Cimalla, V. Lebedev, G. Kittler, M. Himmerlich, S. Krischok, J. A. Schaefer, M. Gebinoga, A. Schober, T. Friedrich and O. Ambacher, *Materwiss. Werkst.*, 2006, **37**, 919–923.
41 S. J. Wilkins, M. Greenough, C. Arellano, T. Paskova and A. Ivanisevic, *Langmuir*, 2014, **30**, 2038–2046.
42 F. L. M. Khir, M. Myers, A. Podolska, T. M. Sanders, M. V. Baker, B. D. Nener and G. Parish, *Appl. Surf. Sci.*, 2014, **314**, 850–857.
43 M. Stutzmann, J. A. Garrido, M. Eickhoff and M. S. Brandt, *Phys. Status Solidi A*, 2006, **203**, 3424–3437.
44 J. Goddard and D. Erickson, *Anal. Bioanal. Chem.*, 2009, **394**, 469–479.
45 B. Baur, J. Howgate, H. G. von Ribbeck, Y. Gawlina, V. Bandalo, G. Steinhoff, M. Stutzmann and M. Eickhoff, *Appl. Phys. Lett.*, 2006, **89**, 183901.
46 J. Lopez-Gejo, A. Navarro-Tobar, A. Arranz, C. Palacio, E. Munoz and G. Orellana, *ACS Appl. Mater. Interfaces*, 2011, **3**, 3846–3854.
47 C.-W. Hsu, A. Ganguly, C.-P. Chen, C.-C. Kuo, P. P. Paskov, P. O. Holtz, L.-C. Chen and K.-H. Chen, *J. Appl. Phys.*, 2011, **109**, 053523.
48 C.-F. Chen, C.-L. Wu and S. Gwo, *Appl. Phys. Lett.*, 2006, **89**, 252109.
49 X. J. Wen, M. L. Schuette, S. K. Gupta, T. R. Nicholson, S. C. Lee and W. Lu, *IEEE Sens. J.*, 2011, **11**, 1726–1735.
50 A. Ganguly, C. P. Chen, Y. T. Lai, C. C. Kuo, C. W. Hsu, K. H. Chen and L. C. Chen, *J. Mater. Chem.*, 2009, **19**, 928–933.
51 A. Arranz, C. Palacio, D. Garcia-Fresnadillo, G. Orellana, A. Navarro and E. Munoz, *Langmuir*, 2008, **24**, 8667–8671.
52 B. Baur, G. Steinhoff, J. Hernando, O. Purrucker, M. Tanaka, B. Nickel, M. Stutzmann and M. Eickhoff, *Appl. Phys. Lett.*, 2005, **87**, 263901.
53 B. S. Simpkins, K. M. Mccoy, L. J. Whitman and P. E. Pehrsson, *Nanotechnology*, 2007, **18**, 355301.
54 C. S. Chiu, H. M. Lee and S. Gwo, *Langmuir*, 2010, **26**, 2969–2974.
55 C.-S. Chiu, H.-M. Lee, C.-T. Kuo and S. Gwo, *Appl. Phys. Lett.*, 2008, **93**, 163106.
56 J. Lopez-Gejo, A. Arranz, A. Navarro, C. Palacio, E. Munoz and G. Orellana, *J. Am. Chem. Soc.*, 2010, **132**, 1746–1747.
57 J. Howgate, S. J. Schoell, M. Hoeb, W. Steins, B. Baur, S. Hertrich, B. Nickel, I. D. Sharp, M. Stutzmann and M. Eickhoff, *Adv. Mater.*, 2010, **22**, 2632–2636.
58 T. Cao, A. F. Wang, X. M. Liang, H. Y. Tang, G. W. Auner, S. O. Salley and K. Y. S. Ng, *Biotechnol. Bioeng.*, 2007, **98**, 1109–1122.
59 T. Cao, A. Wang, X. Liang, H. Tang, G. W. Auner, S. O. Salley and K. Y. Ng, *Colloids Surf., B*, 2008, **63**, 176–182.

60 R. Stine, B. S. Simpkins, S. P. Mulvaney, L. J. Whitman and C. R. Tamanaha, *Appl. Surf. Sci.*, 2010, **256**, 4171–4175.
61 A. Simon, T. Cohen-Bouhacina, M. C. Porte, J. P. Aime and C. Baquey, *J. Colloid. Interface Sci.*, 2002, **251**, 278–283.
62 B. S. Kang, H. T. Wang, T. P. Lele, Y. Tseng, F. Ren, S. J. Pearton, J. W. Johnson, P. Rajagopal, J. C. Roberts, E. L. Piner and K. J. Linthicum, *Appl. Phys. Lett.*, 2007, **91**, 112106.
63 K. H. Chen, B. S. Kang, H. T. Wang, T. P. Lele, F. Ren, Y. L. Wang, C. Y. Chang, S. J. Pearton, D. M. Dennis, J. W. Johnson, P. Rajagopal, J. C. Roberts, E. L. Piner and K. J. Linthicum, *Appl. Phys. Lett.*, 2008, **92**, 192103.
64 B. S. Kang, H. T. Wang, F. Ren, S. J. Pearton, T. E. Morey, D. M. Dennis, J. W. Johnson, P. Rajagopal, J. C. Roberts, E. L. Piner and K. J. Linthicum, *Appl. Phys. Lett.*, 2007, **91**, 252103.
65 Y.-L. Wang, B. H. Chu, C. Y. Chang, C. F. Lo, S. J. Pearton, A. Dabiran, P. P. Chow and F. Ren, *Sens. Actuators, B*, 2010, **146**, 349–352.
66 Y.-L. Wang, B. H. Chu, K. H. Chen, C. Y. Chang, T. P. Lele, G. Papadi, J. K. Coleman, B. J. Sheppard, C. F. Dungen, S. J. Pearton, J. W. Johnson, P. Rajagopal, J. C. Roberts, E. L. Piner, K. J. Linthicum and F. Ren, *Appl. Phys. Lett.*, 2009, **94**, 243901.
67 T. A. Schuller, M. Kuball, S. E. Flower, T. D. James, J. S. Fossey, D. Marcon, J. Das, S. Degroot, M. Germain and A. Sarua, *Sens. Actuators. B*, 2011, **160**, 1078–1081.
68 T. Ito, S. M. Forman, C. Cao, F. Li, C. R. Eddy, M. A. Mastro, R. T. Holm, R. L. Henry, K. L. Hohn and J. H. Edgar, *Langmuir*, 2008, **24**, 6630–6635.
69 H. Kim, P. E. Colavita, P. Paoprasert, P. Gopalan, T. F. Kuech and R. J. Hamers, *Surf. Sci.*, 2008, **602**, 2382–2388.
70 B. S. Simpkins, S. Hong, R. Stine, A. J. Makinen, N. D. Theodore, M. A. Mastro, C. R. Eddy and P. E. Pehrsson, *J Phys. D: Appl. Phys.*, 2010, **43**, 015303.
71 F. Li, E. Shishkin, M. A. Mastro, J. K. Hite, C. R. Eddy Jr., J. H. Edgar and T. Ito, *Langmuir*, 2010, **26**, 10725–10730.
72 D. J. Guo, A. I. Abdulagatov, D. M. Rourke, K. A. Bertness, S. M. George, Y. C. Lee and W. Tan, *Langmuir*, 2010, **26**, 18382–18391.
73 H. Kim, P. E. Colavita, K. M. Metz, B. M. Nichols, B. Sun, J. Uhlrich, X. Y. Wang, T. F. Kuech and R. J. Hamers, *Langmuir*, 2006, **22**, 8121–8126.
74 M. S. Makowski, D. Y. Zemlyanov and A. Ivanisevic, *Appl. Surf. Sci.*, 2011, **257**, 4625–4632.
75 T. Schubert, G. Steinhoff, H. G. von Ribbeck, M. Stutzmannn, M. Eickhoff and M. Tanaka, *Eur. Phys. J. E: Soft Matter Biol. Phys.*, 2009, **30**, 233–238.
76 E. Estephan, C. Larroque, F. J. G. Cuisinier, Z. Balint and C. Gergely, *J. Phys. Chem. B*, 2008, **112**, 8799–8805.
77 X. B. Xu, V. Jindal, F. Shahedipour-Sandvik, M. Bergkvist and N. C. Cady, *Appl. Surf. Sci.*, 2009, **255**, 5905–5909.
78 J. Li, C. Qi, Z. Lian, Q. Han, X. Wang, S. Cai, R. Yang and C. Wang, *ACS Appl. Mater. Interfaces*, 2016, **8**, 2511–2516.
79 A. Neogi, J. Li, P. B. Neogi, A. Sarkar and H. Morkoc, *Electron. Lett.*, 2004, **40**, 1605–1606.
80 M. S. Makowski, D. Y. Zemlyanov, J. A. Lindsey, J. C. Bernhard, E. M. Hagen, B. K. Chan, A. A. Petersohn, M. R. Medow, L. E. Wendel, D. F. Chen, J. M. Canter and A. Ivanisevic, *Surf. Sci.*, 2011, **605**, 1466–1475.
81 B. S. Kang, F. Ren, L. Wang, C. Lofton, W. W. Tan, S. J. Pearton, A. Dabiran, A. Osinsky and P. P. Chow, *Appl. Phys. Lett.*, 2005, **87**, 023508.
82 B. H. Chu, B. S. Kang, C. Y. Chang, F. Ren, A. Goh, A. Sciullo, W. S. Wu, J. S. Lin, B. P. Gila, S. J. Pearton, J. W. Johnson, E. L. Piner and K. J. Linthicum, *IEEE Sens. J.*, 2010, **10**, 64–70.
83 Y. Wang and W. Lu, *Phys. Status Solidi A*, 2011, **208**, 1623–1625.
84 R. Thapa, S. Alur, K. Kim, F. Tong, Y. Sharma, M. Kim, C. Ahyi, J. Dai, J. Wook Hong, M. Bozack, J. Williams, A. Son, A. Dabiran and M. Park, *Appl. Phys. Lett.*, 2012, **100**, 232109.
85 C. C. Huang, G. Y. Lee, J. I. Chyi, H. T. Cheng, C. P. Hsu, Y. R. Hsu, C. H. Hsu, Y. F. Huang, Y. C. Sun, C. C. Chen, S. S. Li, J. A. Yeh, D. J. Yao, F. Ren and Y. L. Wang, *Biosens. Bioelectron.*, 2013, **41**, 717–722.
86 T. Anderson, F. Ren, S. Pearton, B. S. Kang, H. T. Wang, C. Y. Chang and J. S. Lin, *Sensors*, 2009, **9**, 4669–4694.
87 S. J. Pearton, F. Ren, Y. L. Wang, B. H. Chu, K. H. Chen, C. Y. Chang, W. Lim, J. S. Lin and D. P. Norton, *Prog. Mater. Sci.*, 2010, **55**, 1–59.
88 C. S. Lee, S. K. Kim and M. Kim, *Sensors*, 2009, **9**, 7111–7131.
89 G. Steinhoff, M. Hermann, W. J. Schaff, L. F. Eastman, M. Stutzmann and M. Eickhoff, *Appl. Phys. Lett.*, 2003, **83**, 177–179.
90 Y. S. Lu, C. C. Huang, J. A. Yeh, C. F. Chen and S. Gwo, *Appl. Phys. Lett.*, 2007, **91**, 202109.
91 B.-H. Chu, H.-W. Lin, S. Gwo, Y.-L. Wang, S. J. Pearton, J. W. Johnson, P. Rajagopal, J. C. Roberts, E. L. Piner, K. J. Linthicuni and F. Ren, *J. Vac. Sci. Technol., B*, 2010, **28**, L5.
92 S. C. Hung, Y. L. Wang, B. Hicks, S. J. Pearton, D. M. Dennis, F. Ren, J. W. Johnson, P. Rajagopal, J. C. Roberts, E. L. Piner, K. J. Linthicum and G. C. Chi, *Appl. Phys. Lett.*, 2008, **92**, 193903.
93 M. J. Schoning and A. Poghossian, *Analyst*, 2002, **127**, 1137–1151.
94 Y. L. Wang, B. H. Chu, K. H. Chen, C. Y. Chang, T. P. Lele, Y. Tseng, S. J. Pearton, J. Ramage, D. Hooten, A. Dabiran, P. P. Chow and F. Ren, *Appl. Phys. Lett.*, 2008, **93**, 262101.
95 B. H. Chu, C. Y. Chang, K. Kroll, N. Denslow, Y.-L. Wang, S. J. Pearton, A. M. Dabiran, A. M. Wowchak, B. Cui, P. P. Chow and F. Ren, *Appl. Phys. Lett.*, 2010, **96**, 013701.
96 S. Linkohr, S. Schwarz, S. Krischok, P. Lorenz, V. Cimalla, C. Nebel and O. Ambacher, *Phys. Status Solidi C*, 2010, **7**, 1810–1813.
97 G. Steinhoff, B. Baur, G. n. Wrobel, S. Ingebrandt, A. Offenhäusser, A. Dadgar, A. Krost, M. Stutzmann and M. Eickhoff, *Appl. Phys. Lett.*, 2005, **86**, 033901.

98 C. Z. Zhu, G. H. Yang, H. Li, D. Du and Y. H. Lin, *Anal. Chem.*, 2015, **87**, 230–249.
99 N. A. Chaniotakis, Y. Alifragis, G. Konstantinidis and A. Georgakilas, *Anal. Chem.*, 2004, **76**, 5552–5556.
100 Y. Alifragis, G. Konstantinidis, A. Georgakilas and N. Chaniotakis, *Electroanalysis*, 2005, **17**, 527–531.
101 C. P. Chen, A. Ganguly, C. H. Wang, C. W. Hsu, S. Chattopadhyay, Y. K. Hsu, Y. C. Chang, K. H. Chen and L. C. Chen, *Anal. Chem.*, 2009, **81**, 36–42.
102 J. L. Arlett, E. B. Myers and M. L. Roukes, *Nat. Nanotechnol.*, 2011, **6**, 203–215.
103 Y. C. Weng, F. F. Delgado, S. Son, T. P. Burg, S. C. Wasserman and S. R. Manalis, *Lab Chip*, 2011, **11**, 4174–4180.
104 R. Datar, S. Kim, S. Jeon, P. Hesketh, S. Manalis, A. Boisen and T. Thundat, *MRS Bull.*, 2009, **34**, 449–454.
105 K. Lange, B. E. Rapp and M. Rapp, *Anal. Bioanal. Chem.*, 2008, **391**, 1509–1519.
106 M. I. Rocha-Gaso, C. March-Iborra, A. Montoya-Baides and A. Arnau-Vives, *Sensors*, 2009, **9**, 5740–5769.
107 O. Ambacher, B. Foutz, J. Smart, J. R. Shealy, N. G. Weimann, K. Chu, M. Murphy, A. J. Sierakowski, W. J. Schaff, L. F. Eastman, R. Dimitrov, A. Mitchell and M. Stutzmann, *J. Appl. Phys.*, 2000, **87**, 334–344.
108 B. S. Kang, S. Kim, J. Kim, F. Ren, K. Baik, S. J. Pearton, B. P. Gila, C. R. Abernathy, C. C. Pan, G. T. Chen, J. I. Chyi, V. Chandrasekaran, M. Sheplak, T. Nishida and S. N. G. Chu, *Appl. Phys. Lett.*, 2003, **83**, 4845–4847.
109 M. Placidi, J. C. Moreno, P. Godignon, N. Mestres, E. Frayssinet, F. Semond and C. Serre, *Sens. Actuators, A*, 2009, **150**, 64–68.
110 V. Cimalla, F. Niebelschuetz, K. Tonisch, C. Foerster, K. Brueckner, I. Cimalla, T. Friedrich, J. Pezoldt, R. Stephan, M. Hein and O. Ambacher, *Sens. Actuators, B*, 2007, **126**, 24–34.
111 K. Y. Wong, W. Tang, K. M. Lau and K. J. Chen, *Appl. Phys. Lett.*, 2007, **90**, 213506.
112 X. D. Fan, I. M. White, S. I. Shopova, H. Y. Zhu, J. D. Suter and Y. Z. Sun, *Anal. Chim. Acta*, 2008, **620**, 8–26.
113 J. N. Anker, W. P. Hall, O. Lyandres, N. C. Shah, J. Zhao and R. P. Van Duyne, *Nat. Mater.*, 2008, **7**, 442–453.
114 S. Chattopadhyay, S. C. Shi, Z. H. Lan, C. F. Chen, K. H. Chen and L. C. Chen, *J. Am. Chem. Soc.*, 2005, **127**, 2820–2821.
115 K. Agnieszka, D. Igor, L. W. Jan, W. Jacek, G. Sylwester, S. Volodymyr, F. Marcin, S. Marta, S. Tadeusz, P. Sylwester and H. Robert, *J. Mater. Chem.*, 2011, **21**, 8662–8669.
116 J. Wallys, J. Teubert, F. Furtmayr, D. M. Hofmann and M. Eickhoff, *Nano Lett.*, 2012, **12**, 6180–6186.
117 B. S. Kang, H. T. Wang, F. Ren, M. Hlad, B. P. Gila, C. R. Abernathy, S. J. Pearton, C. Li, Z. N. Low, J. Lin, J. W. Johnson, P. Rajagopal, J. C. Roberts, E. L. Piner and K. J. Linthicum, *J. Electron. Mater.*, 2007, **37**, 550–553.
118 C. P. Chen, A. Ganguly, C. Y. Lu, T. Y. Chen, C. C. Kuo, R. S. Chen, W. H. Tu, W. B. Fischer, K. H. Chen and L. C. Chen, *Anal. Chem.*, 2011, **83**, 1938–1943.
119 B. S. Kang, F. Ren, B. P. Gila, C. R. Abernathy and S. J. Pearton, *Appl. Phys. Lett.*, 2004, **84**, 1123–1125.
120 O. Kryliouk, H. J. Park, H. T. Wang, B. S. Kang, T. J. Anderson, F. Ren and S. J. Pearton, *J. Vac. Sci. Technol., B*, 2005, **23**, 1891–1894.
121 J. Schalwig, G. Muller, M. Eickhoff, O. Ambacher and M. Stutzmann, *Sens. Actuators, B*, 2002, **87**, 425–430.
122 O. Weidemann, P. K. Kandaswamy, E. Monroy, G. Jegert, M. Stutzmann and M. Eickhoff, *Appl. Phys. Lett.*, 2009, **94**, 113108.
123 Y. Huang, X. F. Duan, Q. Q. Wei and C. M. Lieber, *Science*, 2001, **291**, 630–633.
124 Y. L. Liu, J. H. Chung, W. K. Liu and R. S. Ruoff, *J. Phys. Chem. B*, 2006, **110**, 14098–14106.
125 T. H. Kim, S. Y. Lee, N. K. Cho, H. K. Seong, H. J. Choi, S. W. Jung and S. K. Lee, *Nanotechnology*, 2006, **17**, 3394–3399.
126 J. Yao, H. Yan and C. M. Lieber, *Nat. Nanotechnol.*, 2013, **8**, 329–335.
127 Y. Z. Long, M. Yu, B. Sun, C. Z. Gu and Z. Y. Fan, *Chem. Soc. Rev.*, 2012, **41**, 4560–4580.
128 M. C. P. Wang and B. D. Gates, *Mater. Today*, 2009, **12**, 34–43.
129 D. Tsivion, M. Schvartzman, R. Popovitz-Biro, P. von Huth and E. Joselevich, *Science*, 2011, **333**, 1003–1007.
130 L. Goren-Ruck, D. Tsivion, M. Schvartzman, R. Popovitz-Biro and E. Joselevich, *ACS Nano*, 2014, **8**, 2838–2847.
131 G. Zheng, F. Patolsky, Y. Cui, W. U. Wang and C. M. Lieber, *Nat. Biotechnol.*, 2005, **23**, 1294–1301.
132 S. J. Pearton, B. S. Kang, S. Kim, F. Ren, B. P. Gila, C. R. Abernathy, J. Lin and S. N. G. Chu, *J. Phys.: Condens. Matter*, 2004, **16**, R961–R994.
133 I. Cimalla, F. Will, K. Tonisch, M. Niebelschütz, V. Cimalla, V. Lebedev, G. Kittler, M. Himmerlich, S. Krischok, J. A. Schaefer, M. Gebinoga, A. Schober, T. Friedrich and O. Ambacher, *Sens. Actuators, B*, 2007, **123**, 740–748.
134 B. S. Kang, H. T. Wang, F. Ren and S. J. Pearton, *J. Appl. Phys.*, 2008, **104**, 031101.
135 R.-S. Chen, H.-Y. Chen, C.-Y. Lu, K.-H. Chen, C.-P. Chen, L.-C. Chen and Y.-J. Yang, *Appl. Phys. Lett.*, 2007, **91**, 223106.
136 J. Song and W. Lu, *Appl. Phys. Lett.*, 2006, **89**, 223503.
137 B. S. Kang, H. T. Wang, L. C. Tien, F. Ren, B. P. Gila, D. P. Norton, C. R. Abernathy, J. S. Lin and S. J. Pearton, *Sensors*, 2006, **6**, 643–666.
138 O. Weidemann, M. Hermann, G. Steinhoff, H. Wingbrant, A. Lloyd Spetz, M. Stutzmann and M. Eickhoff, *Appl. Phys. Lett.*, 2003, **83**, 773–775.
139 S. W. Ryter and L. E. Otterbein, *Bioessays*, 2004, **26**, 270–280.
140 C.-F. Lo, L. Liu, B.-H. Chu, F. Ren, S. J. Pearton, S. Doré, C.-H. Hsu, J. Kim, A. M. Dabiran and P. P. Chow, *J. Vac. Sci. Technol., B*, 2012, **30**, 010606.
141 S. C. Hung, W. Y. Woon, S. M. Lan, F. Ren and S. J. Pearton, *Appl. Phys. Lett.*, 2013, **103**, 083506.

142 C. F. Lo, Y. Xi, L. Liu, S. J. Pearton, S. Doré, C. H. Hsu, A. M. Dabiran, P. P. Chow and F. Ren, *Sens. Actuators, B*, 2013, **176**, 708–712.
143 C. Y. Chang, B. S. Kang, H. T. Wang, F. Ren, Y. L. Wang, S. J. Pearton, D. M. Dennis, J. W. Johnson, P. Rajagopal, J. C. Roberts, E. L. Piner and K. J. Linthicum, *Appl. Phys. Lett.*, 2008, **92**, 232102.
144 Y.-L. Wang, C. Y. Chang, W. Lim, S. J. Pearton, D. P. Norton, B. H. Chu, C. F. Lo, F. Ren, J. W. Johnson, P. Rajagopal, J. C. Roberts, E. L. Piner and K. J. Linthicum, *J. Vac. Sci. Technol., B*, 2010, **28**, 376–379.
145 A. Podolska, D. Broxtermann, J. Malindretos, G. A. Umana-Membreno, S. Keller, U. K. Mishra, A. Rizzi, B. D. Nener and G. Parish, *IEEE Sens. J.*, 2015, **15**, 5320–5326.
146 A. B. Encabo, J. Howgate, M. Stutzmann, M. Eickhoff and M. A. Sánchez-García, *Sens. Actuators, B*, 2009, **142**, 304–307.
147 Y.-S. Lu, C.-L. Ho, J. A. Yeh, H.-W. Lin and S. Gwo, *Appl. Phys. Lett.*, 2008, **92**, 212102.
148 J. D. Li, J. J. Cheng, B. Miao, X. W. Wei, J. Xie, J. C. Zhang, Z. Q. Zhang, H. W. Li and D. M. Wu, *Microsyst. Technol.*, 2015, **21**, 1489–1494.
149 H. H. Lee, M. Bae, S.-H. Jo, J.-K. Shin, D. H. Son, C.-H. Won and J.-H. Lee, *Sens. Actuators, B*, 2016, **234**, 316–323.
150 Y.-L. Wang, B. H. Chu, K. H. Chen, C. Y. Chang, T. P. Lele, Y. Tseng, S. J. Pearton, J. Ramage, D. Hooten, A. Dabiran, P. P. Chow and F. Ren, *Appl. Phys. Lett.*, 2008, **93**, 262101.
151 B. H. Chu, C. Y. Chang, K. Kroll, N. Denslow, Y.-L. Wang, S. J. Pearton, J. Lin, A. M. Dabiran, A. M. Wowchak, B. Cui, P. P. Chow, J. W. Johnson, P. Rajagopal, J. C. Roberts, E. L. Piner, K. J. Linthicum and F. Ren, *Phys. Status Solidi C*, 2011, **8**, 2486–2488.
152 Y. W. Kang, G. Y. Lee, J. I. Chyi, C. P. Hsu, Y. R. Hsu, C. H. Hsu, Y. F. Huang, Y. C. Sun, C. C. Chen, S. C. Hung, F. Ren, J. A. Yeh and Y. L. Wang, *Appl. Phys. Lett.*, 2013, **102**, 173704.
153 M. S. Makowski, I. Bryan, Z. Sitar, C. Arellano, J. Xie, R. Collazo and A. Ivanisevic, *Appl. Phys. Lett.*, 2013, **103**, 1–5.
154 J. D. Li, J. J. Cheng, B. Miao, X. W. Wei, J. Xie, J. C. Zhang, Z. Q. Zhang, H. W. Li and D. M. Wu, *Microsyst. Technol.*, 2015, **21**, 1489–1494.
155 P. Sahoo, S. Suresh, S. Dhara, G. Saini, S. Rangarajan and A. K. Tyagi, *Biosens. Bioelectron.*, 2013, **44**, 164–170.
156 N. Espinosa, S. U. Schwarz, V. Cimalla and O. Ambacher, *Sens. Actuators, B*, 2015, **210**, 633–639.
157 A. Podolska, L. C. Hool, K. D. G. Pfleger, U. K. Mishra, G. Parish and B. D. Nener, *Sens. Actuators, B*, 2013, **177**, 577–582.
158 M. Gebinoga, P. Mai, M. Donahue, M. Kittler, I. Cimalla, B. Lubbers, M. Klett, V. Lebedev, L. Silveira, S. Singh and A. Schober, *J. Neurosci. Methods*, 2012, **206**, 195–199.
159 G. M. Muntze, E. Pouokam, J. Steidle, W. Schafer, A. Sasse, K. Roth, M. Diener and M. Eickhoff, *Biosens. Bioelectron.*, 2016, **77**, 1048–1054.
160 H. Witte, T. Lippelt, C. Warnke, A. Dadgar, M. J. B. Hauser and A. Krost, *J. Phys. D: Appl. Phys.*, 2014, **47**, 425401.
161 B. Lübbers, G. Kittler, P. Ort, S. Linkohr, D. Wegener, B. Baur, M. Gebinoga, F. Weise, M. Eickhoff, S. Maroldt, A. Schober and O. Ambacher, *Phys. Status Solidi C*, 2008, **5**, 2361–2363.
162 S. Krishna, S. A. Boren and E. A. Balas, *Telemed. J. E-Health*, 2009, **15**, 231–240.
163 D. N. Breslauer, R. N. Maamari, N. A. Switz, W. A. Lam and D. A. Fletcher, *PLoS One*, 2009, **4**, e6320.
164 Q. Wang, S. Savage, S. Persson, B. Noharet, S. Junique, J. Y. Andersson, V. Liuolia and S. Marcinkevicius, *Proc. SPIE*, 2009, **7216**, 721627.
165 J. Schalwig, G. Muller, O. Ambacher and M. Stutzmann, *Phys. Status Solidi A*, 2001, **185**, 39–45.
166 J. Schalwig, G. Muller, M. Eickhoff, O. Ambacher and M. Stutzmann, *Mater. Sci. Eng., B*, 2002, **93**, 207–214.
167 M. S. Makowski, I. Bryan, Z. Sitar, C. Arellano, J. Q. Xie, R. Collazo and A. Ivanisevic, *Appl. Phys. Lett.*, 2013, **103**, 013701.
168 B. S. Kang, S. J. Pearton, J. J. Chen, F. Ren, J. W. Johnson, R. J. Therrien, P. Rajagopal, J. C. Roberts, E. L. Piner and K. J. Linthicum, *Appl. Phys. Lett.*, 2006, **89**, 122102.
169 K. Brueckner, F. Niebelschuetz, K. Tonisch, C. Foerster, V. Cimalla, R. Stephan, J. Pezoldt, T. Stauden, O. Ambacher and M. A. Hein, *Phys. Status Solidi A*, 2011, **208**, 357–376.
170 T. A. Schuller, M. Kuball, S. E. Flower, T. D. James, J. S. Fossey, D. Marcon, J. Das, S. Degroot, M. Germain and A. Sarua, *Sens. Actuat., B*, 2011, **160**, 1078–1081.